

Tests of the parametrizations of Fragmentation Functions using data on inclusive pion and kaon production in unpolarized pp collisions from the STAR collaboration and at the NICA project.

D. Kotlorz^{a†}

Bogoliubov Laboratory of Theoretical Physics, JINR, 141980 Dubna, Russia

E. Christova[‡]

*Institute for Nuclear Research and Nuclear Energy,
Bulgarian Academy of Sciences, Tzarigradsko chaussée 72, 1784 Sofia, Bulgaria*

E. Leader[§]

Imperial College London, London SW7 2AZ, United Kingdom

(Dated: September 12, 2023)

The goal of this study is to check which, if any, of the published versions of the pion and kaon fragmentation functions is compatible with the STAR data on semi-inclusive pion and kaon production in proton-proton collisions, and on the basis of this analysis to make reliable predictions for the p_T spectra of the pions and kaons in inclusive pion and kaon production at the future NICA proton-proton collider.

The calculations are carried out in next-to-leading order (NLO) of perturbative quantum chromodynamics (pQCD), using the well tested CTEQ6 parton distributions. We consider the following pion and kaon fragmentation functions (FFs) – DSEHS-14 [1], DSEHS-17 [2], LSS-15 [3], HKNS-07 [4] and AKK-08 [5]. Our analysis shows that within the experimental errors all tested sets of fragmentation functions provide a good fit to STAR data at the c.m. energy $\sqrt{S} = 200$ GeV, and the best ones are both LSS-15 and DSEHS-14 for pions and DSEHS-17 for kaons. From comparison of the LO and NLO results it is clear that the latter fit data much better, specially in the region of small p_T . The NLO cross sections are also less scale- Q^2 dependent, where $p_T/2 \leq Q \leq 2p_T$, than the LO ones.

In order to make predictions for NICA energies, we compare the NLO pQCD results with the existing experimental BES STAR data on semi-inclusive hadron production in the most peripheral Au+Au collisions where the nuclear effects can be neglected. The comparison for lower energy scales, like at NICA, shows that a purely pQCD approach is inadequate and suggests the necessity to take into account also higher-order effects of initial-state soft-gluon radiation. Nevertheless, these data on the p_T spectra of π^+ , K^+ and also the ratios π^-/π^+ and K^-/K^+ seem favour LSS-15 and DSEHS-14 FFs for pions and DSEHS-17 for kaons, similarly as at the energy scale $\sqrt{S} = 200$ GeV.

I. INTRODUCTION

Study of the spectra of identified hadrons at high p_T in pp collisions is based on model calculations in perturbative quantum chromodynamics (pQCD) [6]. Both in leading order (LO) [7–11] and in next-to-leading order (NLO) [12–14] of pQCD calculations, inclusive production of single hadrons is described in terms of parton distribution functions (PDFs), parton-parton interaction cross sections calculated in the Standard Model (SM), and fragmentation functions. The PDFs are fairly well known, while on the contrary, the flavor-separated quark and gluon FFs, being relatively new objects, required for a quantitative description of hard scattering processes involving identified light hadrons in the final-state, are not so well constrained. At present there are several sets of FFs that fairly well describe data, but nevertheless differ quite a lot in different kinematic regions. Most directly the FFs have been extracted from one-hadron production in electron-positron collisions. However, this process in principle, cannot distinguish the quark and anti-quark FFs and information only about $D_{q+\bar{q}}^h$ is obtained. In order to obtain separate quark and anti-quark FFs, one-hadron semi-inclusive lN and pp processes play an essential role. However, as the hadron structure enters in comparing theoretical calculations with experimental data, different model assumptions have to be made. One of the goals in the experimental measurements by the STAR collaboration of pions and kaons at high p_T in pp collisions is to provide more information on the FFs.

^a On leave of absence from Department of Physics, Opole University of Technology, 45-758 Opole, Proszkowska 76, Poland

[†] dorota@theor.jinr.ru

[‡] echristo@inrne.bas.bg

[§] e.leader@imperial.ac.uk

In this paper, based fully on pQCD and taking into account all partonic cross sections in NLO, we calculate the hadronic p_T -spectra of the final pions and kaons in single hadron production in pp collisions in the high p_T region, and compare it to the STAR data from 2006 [15], 2007 [16] and 2012 [17]. We use various published parametrizations for the FFs: HKNS-07 [4], AKK-08 [5], DSEHS-14 [1], DSEHS-17 [2] and LSS-15 [3], aiming to obtain constraints on the available sets of FFs from the sensitivity of STAR data to the used FFs. We use CTEQ6 parametrization for PDFs [18]. Using these data to constrain the FFs, should lead to more reliable predictions for future measurements. In particular we consider the effect on data expected from the future NICA accelerator.

Our analysis is partially based on the model independent approach of the difference cross sections of h^+ and h^- -production, developed in [19]. It suggests that, both in e^+e^- , SIDIS and proton-proton collisions, if instead of the X-sections $d\sigma_{e^+e^-}^h$, $d\sigma_N^h$ and $d\sigma_{pp}^h$ for inclusive production of hadrons and their antiparticles, one deals with their differences, i.e. with $d\sigma_{e^+e^-}^{h-\bar{h}}$, $d\sigma_N^{h-\bar{h}}$ and $d\sigma_{pp}^{h-\bar{h}} \equiv d\sigma_{pp}^h - d\sigma_{pp}^{\bar{h}}$, one determines directly the non-singlet (NS) combinations of FFs $D_q^{h-\bar{h}} = D_{q_v}^h$. This result follows solely from charge-conjugation invariance of the strong interactions without any model assumptions about the sea-quarks or favoured and unfavoured fragmentation functions.

The STAR Collaboration has presented data for pions and kaons. In comparing with the data we make two simplifications in our formula for the spectra of the pions and the kaons. 1) We use $s = \bar{s}$ for the strange quark PDFs. Note that this is not an assumption but follows from the strong limit $|s - \bar{s}| < 0.025$ obtained in neutrino experiments [20] and implies that the contribution from terms proportional to $s - \bar{s}$ will be within the experimental errors and thus negligible. 2) We assume SU(2) isospin symmetry of the strong interactions. The theoretical framework for inclusive production of single hadrons in pp collisions is presented in Section II, and the expressions for the difference cross sections and the conditions under which they have been derived are given in Section III. The comparison of our results to the STAR data is presented in Section IV. Here, we also compare the results obtained within NLO and LO approaches and study the scale dependence of the cross sections for the charged hadrons at LO and NLO where the scale Q may vary from $p_T/2$ to $2p_T$.

Unfortunately we cannot take advantage of the very simple expressions derived in Section III for the cross-section differences, because the experimental errors on these are too large.

Based on the obtained results for the FFs, we calculate the expected p_T -spectra of the pions and kaons produced in pp collisions at the kinematics of the planned NICA accelerator. We compare the theoretical NLO pQCD predictions with the experimental BES STAR data on semi-inclusive pion and kaon production in the most peripheral Au+Au collisions, where nuclear effects can be neglected [21, 22], at energies $\sqrt{S} = 11.5$ and 27 GeV, specific to NICA [23, 24], and show that at such low energy scales and the correspondingly low values of p_T , the contributions to the inclusive cross section for hadron production coming from various soft processes become essential. Therefore, the perturbative QCD approach should be here treated with caution. This is discussed in Section V. We summarize the obtained results in a Conclusion.

II. THE THEORETICAL FRAMEWORK FOR $pp \rightarrow h + X$

We consider the process:

$$p(P_A) + p(P_B) \rightarrow h(P^h) + X \quad (1)$$

The basic concept [6] underlying the theoretical analysis of most high energy interactions is the factorization theorem, which states that the cross-section for large momentum-transfer reactions may be factorized into long-distance pieces that contain the desired information on the structure of the nucleon in terms of its parton densities such as $q(x)$ and fragmentation functions $D_q^h(z)$, and short-distance parts which describe the hard interactions of the partons. The strength of this interaction is controlled by the running strong-interaction coupling constant α_s evaluated at a large scale associated with the hard interaction which we denote by Q^2 . The effective coupling constant falls logarithmically with increasing Q^2 , $\alpha_s(Q^2) \sim 1/\ln(Q^2/\Lambda_{\text{QCD}}^2)$, enabling the perturbative QCD analysis for the hard-scale $Q \gg \Lambda_{\text{QCD}}$, where $\Lambda_{\text{QCD}} \sim 0.3$ GeV. The two crucial points here are, on one hand the long-distance contributions are universal, i.e., they are the same in any inelastic reaction under consideration, and on the other hand the short-distance pieces depend only on the large scales related to the large momentum transfer in the overall reaction and, therefore, can be evaluated using QCD perturbation theory.

Calculations in LO, Eq. (1), have been considered and compared to data in several papers in [7–11]. The first calculations beyond LO, at (α_s^3) order in perturbative QCD, that include the virtual corrections in the $2 \rightarrow 2$ and the $2 \rightarrow 3$ partonic subprocesses, have been calculated in [12–14], and the full $\mathcal{O}(\alpha_s^3)$ radiative NLO corrections are presented in [14].

The results presented for the unpolarized cross section for $pp \rightarrow \pi + X$ at $\sqrt{S} = 200$ GeV, that are well described by the NLO QCD calculation [25], provide confidence that the theoretical framework based on perturbative-QCD

hard scattering is adequate.

Here we consider cross sections $pp \rightarrow h^\pm + X$ and also difference cross sections $\sigma(pp \rightarrow h^+ + X) - \sigma(pp \rightarrow h^- + X)$. The calculations are done in NLO in the QCD improved parton model following the approach of [14] which include all parton subprocesses involving quarks and gluons. In our numerical analysis, we have adapted the INCNLO inclusive hadron production code [26] and also a code for calculating the fragmentation functions [4].

In the simple parton model process (1) proceeds via the $2 \rightarrow 2$ partonic subprocesses:

$$q_a(p_a) + q_b(p_b) \rightarrow c(p_c) + d(p_d) \quad (2)$$

where q_a, q_b and c, d can be either quarks or gluons. In what follows all kinematic variables refer to the CM of the pp collision. The expression for the cross section for $pp \rightarrow hX$ in the c.m.s. of pp has the factorized form:

$$E^h \frac{d\sigma_{pp}^h}{d^3P^h} = \frac{1}{\pi} \sum_{ab \rightarrow cd} \int_{x_{a,min}}^1 dx_a \int_{x_{b,min}}^1 dx_b \frac{1}{z} \times \\ \times \left\{ q_a(x_a) q_b(x_b) \left[\frac{d\hat{\sigma}_{ab}^{cd}}{dt} D_c^h(z) + \frac{d\hat{\sigma}_{ab}^{cd}}{du} D_d^h(z) \right] + q_a(x_b) q_b(x_a) \left[\frac{d\hat{\sigma}_{ab}^{cd}}{du} D_c^h(z) + \frac{d\hat{\sigma}_{ab}^{cd}}{dt} D_d^h(z) \right] \right\}. \quad (3)$$

where $d\hat{\sigma}_{ab}^{cd}$ are the Born cross sections to order α_s^2 and the parton densities and FFs are scale independent, $z = E^h/E_c$, and where

$$\frac{d\hat{\sigma}_{ab}^{cd}}{dt} \equiv \frac{d\hat{\sigma}_{ab}^{cd}}{dt}(s, t, u), \quad \frac{d\hat{\sigma}_{ab}^{cd}}{du} \equiv \frac{d\hat{\sigma}_{ab}^{cd}}{du}(s, u, t). \quad (4)$$

As usual x_a (x_b) is the fraction of the proton momentum P_A (P_B) carried by the parton q_a (q_b), collinear to the momentum of the initial hadron A (B).

In the QCD improved parton model, when QCD corrections are included, the factorized form of (3) is preserved and the PDFs and FFs are replaced by Q^2 -dependent distribution functions:

$$q(x) \rightarrow q(x, Q^2), \quad D_q^h(z) \rightarrow D_q^h(z, Q^2), \quad (5)$$

where Q^2 is some relevant large momentum scale. Furthermore, the effective quark-gluon-quark coupling constant α_s becomes the running coupling given at NLO by

$$\alpha_s(Q^2) = \frac{4\pi}{\beta_0 \ln(Q^2/\Lambda_{\text{QCD}}^2)} \left(1 - \frac{\beta_1 \ln \ln(Q^2/\Lambda_{\text{QCD}}^2)}{\beta_0^2 \ln(Q^2/\Lambda_{\text{QCD}}^2)} \right), \quad (6)$$

where $\beta_0 = 11 - 2/3 N_f$ for N_f flavours, $\beta_1 = 102 - 38/3 N_f$ and NLO $\Lambda_{\text{QCD}} = 0.32 \text{ GeV}$. The momentum scale Q^2 is set to the “natural” scale $Q^2 = p_T^2$ [13]. In order to use the PDFs and FFs, known from some other process at some other “input” scale $Q_0^2 = 1 \text{ GeV}^2$, we evolve the PDFs and FFs from Q_0^2 to $Q^2 > Q_0^2$ via the NLO DGLAP-equations. This procedure works well for hard-scale $Q \gg \Lambda_{\text{QCD}}$, typically for Q^2 above $\sim 1 \text{ GeV}^2$, where the short-distance part of the strong interactions is expected to dominate and hence the perturbative QCD methods can be applied.

In our approach when using the difference cross sections, only NS combinations of FFs enter – see for example Eqs. (20) and (29). In this case the DGLAP evolution equations for a given FF is especially simple with no mixing with other FFs.

The Mandelstam variables of the partonic process (2) are:

$$s = (p_a + p_b)^2 = (x_a P_A + x_b P_B)^2 = x_a x_b S \\ t = (p_a - p_c)^2 = (x_a P_A - \frac{P^h}{z})^2 = \frac{x_a}{z} T, \\ u = (p_b - p_c)^2 = (x_b P_B - \frac{P^h}{z})^2 = \frac{x_b}{z} U \quad (7)$$

Here c or d are the fragmenting partons that are assumed collinear to the final hadron h , and everywhere masses are neglected, so that $s + t + u = 0$ holds, which determines the value of z :

$$z = - \frac{x_a T + x_b U}{x_a x_b S} \quad (8)$$

The letters S , T and U stand for the Mandelstam variables of the inclusive hadronic process (1):

$$S = (P_A + P_B)^2 = 2(P_A \cdot P_B) = 4E^2 \quad (9)$$

$$T = (P_A - P^h)^2 = -2(P_A \cdot P^h) = -2EE^h(1 - \cos \theta) \quad (10)$$

$$U = (P_B - P^h)^2 = -2(P_B \cdot P^h) = -2EE^h(1 + \cos \theta) \quad (11)$$

$$p_T^2 = \frac{UT}{S} = (E^h)^2 \sin^2 \theta, \quad (12)$$

where, as mentioned, the kinematic variables refer to the CM of the pp collision; E is the energy of the colliding proton beams. The maximal value of the transverse momentum of a hadron h produced with energy E^h in pp collisions is

$$p_T^{max} = E^h, \text{ at } \theta = \pi/2. \quad (13)$$

Often the p_T -spectra are presented in terms of its relative value $x_T = 2p_T/\sqrt{S}$, where $\sqrt{S}/2 = E$.

The lower limits of integration are determined by the conditions $z < 1$ and $s + t + u = 0$ [9]:

$$x_{a,min} = \frac{-U}{T + S} \quad (14)$$

$$x_{b,min} = \frac{-x_a T}{x_a S + U} \quad (15)$$

There are 8 different $2 \rightarrow 2$ partonic processes that contribute to $d\sigma_{pp}^h$:

$$\begin{aligned} \hat{\sigma}_1 : & \quad q_i q_j \rightarrow q_i q_j, \quad \bar{q}_i \bar{q}_j \rightarrow \bar{q}_i \bar{q}_j, \quad q_i \bar{q}_j \rightarrow q_i \bar{q}_j, i \neq j \\ \hat{\sigma}_2 : & \quad q_i q_i \rightarrow q_i q_i, \quad \bar{q}_i \bar{q}_i \rightarrow \bar{q}_i \bar{q}_i, \\ \hat{\sigma}_3 : & \quad q_i \bar{q}_i \rightarrow q_j \bar{q}_j, \quad i \neq j \\ \hat{\sigma}_4 : & \quad q_i \bar{q}_i \rightarrow q_i \bar{q}_i \\ \hat{\sigma}_5 : & \quad q_i \bar{q}_i \rightarrow gg \\ \hat{\sigma}_6 : & \quad gg \rightarrow q_i \bar{q}_i \\ \hat{\sigma}_7 : & \quad q_i g \rightarrow q_i g \\ \hat{\sigma}_8 : & \quad gg \rightarrow gg \end{aligned} \quad (16)$$

expressions for which can be found in many places. In NLO $\mathcal{O}(\alpha_s^3)$, additional $2 \rightarrow 3$ scattering processes also contribute [12–14].

The contributions of the partonic processes which occur in Eq. (1) are given in Appendix A.

III. THE DIFFERENCE CROSS SECTIONS : $h^+ - h^-$

Here we would like to introduce the idea of the difference cross sections and discuss its possible advantages. We define the difference cross section:

$$\sigma_{pp}^{h^+ - h^-} \equiv \sigma_{pp}^{h^+} - \sigma_{pp}^{h^-}. \quad (17)$$

C-invariance of strong interactions implies:

$$D_g^{h^+ - h^-} = 0, \quad (18)$$

$$D_q^{h^+ - h^-} = -D_{\bar{q}}^{h^+ - h^-} = D_{q_V}^{h^+}. \quad (19)$$

The cross section $\sigma_{pp}^{h^+ - h^-}$ has especially simply form in LO, where, without any assumptions about the sea quark PDFs or the favoured and unfavoured FFs, we obtain:

$$E^h \frac{d\sigma_{pp}^{h^+ - h^-}}{d^3 P^h} = \frac{1}{\pi} \int dx_a dx_b \frac{1}{z} \sum_{q=u,d,s} D_{q_V}^{h^+}(z) (q_V(x_a) L_q(x_b, t, u) + q_V(x_b) L_q(x_a, u, t)), \quad (20)$$

where

$$L_u(x_b, t, u) = (\tilde{d} + \tilde{s})(x_b) \frac{d\hat{\sigma}_1}{dt} + \frac{1}{2} \tilde{u}(x_b) \left[\frac{d\hat{\sigma}_2}{dt} + \frac{d\hat{\sigma}_4}{dt} - \frac{d\hat{\sigma}_4}{du} \right] + g(x_b) \frac{d\hat{\sigma}_7}{dt} \quad (21)$$

$$L_d(x_b, t, u) = (\tilde{u} + \tilde{s})(x_b) \frac{d\hat{\sigma}_1}{dt} + \frac{1}{2} \tilde{d}(x_b) \left[\frac{d\hat{\sigma}_2}{dt} + \frac{d\hat{\sigma}_4}{dt} - \frac{d\hat{\sigma}_4}{du} \right] + g(x_b) \frac{d\hat{\sigma}_7}{dt} \quad (22)$$

$$L_s(x_b, t, u) = (\tilde{u} + \tilde{d})(x_b) \frac{d\hat{\sigma}_1}{dt} + \frac{1}{2} \tilde{s}(x_b) \left[\frac{d\hat{\sigma}_2}{dt} + \frac{d\hat{\sigma}_4}{dt} - \frac{d\hat{\sigma}_4}{du} \right] + g(x_b) \frac{d\hat{\sigma}_7}{dt} \quad (23)$$

and for example

$$L_u(x_a, u, t) = (\tilde{d} + \tilde{s})(x_a) \frac{d\hat{\sigma}_1}{du} + \frac{1}{2} \tilde{u}(x_a) \left[\frac{d\hat{\sigma}_2}{dt} + \frac{d\hat{\sigma}_4}{du} - \frac{d\hat{\sigma}_4}{dt} \right] + g(x_a) \frac{d\hat{\sigma}_7}{du}. \quad (24)$$

In the last formula we have used the fact that $\hat{\sigma}_2$ is symmetric under $t \leftrightarrow u$. Here u_V and d_V are the usual valence quark PDFs:

$$u_V = u - \bar{u}, \quad d_V = d - \bar{d} \quad (25)$$

and we have used the notation:

$$s_V = s - \bar{s}, \quad \bar{q} = q + \bar{q}. \quad (26)$$

Using the strong bound on $(s - \bar{s})$ obtained from neutrino experiments $s_V \leq 0.025$ [20] one may safely neglect the contribution of $s_V D_{s_V}^h$ and we have:

$$E^h \frac{d\sigma_{pp}^{h^+h^-}}{d^3 P^h} = \frac{1}{\pi} \int dx_a dx_b \frac{1}{z} \sum_{q=u,d} D_{q_V}^{h^+}(z) (q_V(x_a) L_q(x_b, t, u) + q_V(x_b) L_q(x_a, u, t)) \quad (27)$$

This implies that the contribution of $(s - \bar{s}) D_s^{h^+h^-}$ is expected to be within the experimental error and negligible, also the large uncertainties in D_s^h should not affect the results for $\sigma_{pp}^{h^+h^-}$.

Note that in LO only 4 partonic cross sections contribute to the difference $d\sigma_{pp}^{h^+h^-}$:

- scattering of flavour-unlike quarks $\hat{\sigma}_1$,
- scattering of flavor-like quarks $\hat{\sigma}_2$ and $\hat{\sigma}_4$ and
- quark-gluon scattering $\hat{\sigma}_7$.

In NLO, the expressions for the difference cross sections are much more complicated as all radiative corrections $\mathcal{O}(\alpha_s^3)$ must be accounted for. Nevertheless, again, one obtains only nonsinglet contributions proportional to $D_{q_V}^{h^+}(z, Q^2)$.

A. The difference cross section for $\pi^+ - \pi^-$

Eq. (20) considerably simplifies for pions if one assumed SU(2) isospin symmetry, as used in all present analyses. It implies:

$$D_u^{\pi^+ - \pi^-} = -D_d^{\pi^+ - \pi^-}, \quad D_s^{\pi^+ - \pi^-} = 0. \quad (28)$$

Then $\sigma_{pp}^{\pi^+ - \pi^-}$ is expressed solely in terms of $D_{u_V}^{\pi^+}$, enhanced by the best known valence-quark u_V :

$$E^\pi \frac{d\sigma_{pp}^{\pi^+ - \pi^-}}{d^3 P^\pi} = \frac{1}{\pi} \int dx_a dx_b \frac{1}{z} D_{u_V}^{\pi^+}(z) \times \\ \times [u_V(x_a) L_u(x_b, t, u) - d_V(x_a) L_d(x_b, t, u) + u_V(x_b) L_u(x_a, u, t) - d_V(x_b) L_d(x_a, u, t)] \quad (29)$$

B. The difference cross section for $K^+ - K^-$

The formula for $\sigma_{pp}^{K^+ - K^-}$ strongly simplifies if we assume:

$$D_d^{K^+ - K^-} = 0 \quad (30)$$

This seems a reasonable physical assumption that follows from the quark content of $K^\pm = (\bar{s}, u)$, (s, \bar{u}) and is used in all current analyses. Then $\sigma_{pp}^{K^+-K^-}$ depends solely on one non-singlet combination of FFs $D_{uV}^{K^+}$, multiplied by the large valence u_V -quark distributions:

$$E^K \frac{d\sigma_{pp}^{K^+-K^-}}{d^3PK} = \frac{1}{\pi} \int dx_a dx_b \frac{1}{z} D_{uV}^{K^+}(z) [u_V(x_a) L_u(x_b, t, u) + u_V(x_b) L_u(x_a, u, t)] \quad (31)$$

This expression may be used as a test for the assumption (30).

C. The difference cross section for K^\pm and K_s^0

If in addition to the charged K^\pm also neutral kaons $K_s^0 = (K^0 + \bar{K}^0)/\sqrt{2}$ are measured, no new FFs are introduced into the cross-sections. This is a consequence of SU(2) isospin symmetry, according to which (K^+, K^0) and (K^-, \bar{K}^0) form isospin doublets, and we have:

$$\begin{aligned} D_u^{K^++K^-}(z, Q^2) &= D_d^{K^0+\bar{K}^0}(z, Q^2) = 2D_d^{K_s^0}(z, Q^2) \\ D_d^{K^++K^-}(z, Q^2) &= D_u^{K^0+\bar{K}^0}(z, Q^2) = 2D_u^{K_s^0}(z, Q^2) \\ D_s^{K^++K^-}(z, Q^2) &= D_s^{K^0+\bar{K}^0}(z, Q^2) = 2D_s^{K_s^0}(z, Q^2). \end{aligned} \quad (32)$$

Note that the first relation involves favoured and unfavoured FFs, while the second – only unfavoured FFs. As explained in [5], due to the nature of the DGLAP evolution, these constraints are independent of Q^2 , as constraints that follow from symmetry should be.

We write Eqs. (32) in the form:

$$D_u^{K^++K^- - 2K_s^0} = -D_d^{K^++K^- - 2K_s^0} = (D_u - D_d)^{K^++K^-} \quad (33)$$

$$D_s^{K^++K^- - 2K_s^0} = D_c^{K^++K^- - 2K_s^0} = D_b^{K^++K^- - 2K_s^0} = D_g^{K^++K^- - 2K_s^0} = 0. \quad (34)$$

Then, as shown in [19], the combination

$$\sigma^{K^+} + \sigma^{K^-} - 2\sigma^{K_s^0} \quad (35)$$

in the three types of inclusive processes, $K = K^\pm, K_s^0$:

$$e^+ + e^- \rightarrow K + X, \quad (36)$$

$$e + N \rightarrow e + K + X, \quad N = p, d, \quad (37)$$

$$p + p \rightarrow K + X, \quad (38)$$

measure the same NS combination of FFs, namely $(D_u - D_d)^{K^++K^-}$. This result relies only on SU(2) invariance for the kaons and does not involve *any* assumptions about PDFs or FFs; it holds in any order in QCD.

For inclusive hadron production, from Eqs. (3) and (33) we obtain:

$$\begin{aligned} E^K \frac{d\sigma_{pp}^{K^++K^- - 2K_s^0}}{d^3PK} &= \frac{1}{\pi} \int dx_a \int dx_b \frac{1}{z} \times \\ &\times \left\{ [\tilde{u}(x_a)[\tilde{d}(x_b) + \tilde{s}(x_b)] - \tilde{d}(x_a)[\tilde{u}(x_b) + \tilde{s}(x_b)]] \frac{d\hat{\sigma}_1}{dt} + \right. \\ &+ \frac{1}{2} [u(x_a)u(x_b) + \bar{u}(x_a)\bar{u}(x_b) - [d(x_a)d(x_b) + \bar{d}(x_a)\bar{d}(x_b)]] \frac{d\hat{\sigma}_2}{dt} + \\ &+ [d(x_a)\bar{d}(x_b) - u(x_a)\bar{u}(x_b)] \left[\frac{d\hat{\sigma}_3}{dt} - \frac{d\hat{\sigma}_4}{dt} \right] + [\tilde{u}(x_a) - \tilde{d}(x_a)]g(x_b) \frac{d\hat{\sigma}_7}{dt} \\ &\left. + [(x_a \leftrightarrow x_b), (t \leftrightarrow u)] \right\} D_{u-d}^{K^++K^-}(z). \end{aligned} \quad (39)$$

Note that $D_q^{h+\bar{h}}$ can be determined directly from $e^+e^- \rightarrow h + X$ and thus without assumptions, which implies that $D_q^{h+\bar{h}}$ should be roughly the same for all sets of FFs. If this appears the case, then use of Eq. (39) to compare the STAR data on $K^+ + K^- - 2K_s^0$ can be used as a test for the consistency of the data with SU(2) invariance.

IV. COMPARISON TO STAR DATA

In this section we study numerically the impact of the different sets of FFs on the p_T -spectra of the final hadrons in inclusive pp -collisions and compare it to STAR data.

Based on the theoretical NLO pQCD-formulas, we examine the sensitivity of the p_T -spectra to the FFs. We use STAR data from 2006, 2007 and 2012 to try to distinguish among the different FFs. First, we compare the cross sections for $d\sigma_{pp}^{h^\pm}$ and $d\sigma_{pp}^{h^+-h^-}$, calculated with different sets for D_q^h , to the measured hadron yield. Second, we try to obtain a fit of the FFs and compare it to the available parametrizations.

Note that there is a principle difference between the commonly used formula for π^\pm -production and the one for $\pi^+ - \pi^-$. In π^\pm production FFs with all flavours D_i^h , $i = g, u, d, s, \bar{u}, \bar{d}, \bar{s}$ enter the cross section, while in the formula for $\pi^+ - \pi^-$ it is only the valence-quark FFs that enter – the non-singlet combinations D_{uV}^h and D_{dV}^h . Note also that, being non-singlets, in their Q^2 -evolution they do not mix with other FFs and this property holds in all orders in QCD.

Finally we use the preferred sets of FFs obtained in the above studies to make predictions for the p_T spectra of the charged pions and kaons produced in inclusive pp collisions at the planned NICA accelerator.

The results are presented separately for final pions and kaons.

We consider the following sets of NLO in pQCD FFs for pions: HKNS-07 [4], AKK-08 [5], DSEHS-14 [1], LSS-15 [3] and for kaons: HKNS-07 [4], AKK-08 [5], DSEHS-17 [2]. These sets of FFs differ by the different processes, whose data they use, and by the used assumptions. Only AKK and DSEHS use the inclusive pp -process as a source of information about the FFs.

We apply NLO approach [14] to STAR data from 2006 [15], 2007 [16] and 2012 [17]. The kinematics of the used measurements of STAR Collaborations in terms of \sqrt{S} , p_T and the rapidity y are:

STAR-2006, π^\pm :

$$\sqrt{S} = 200 \text{ GeV}, \quad 0.3 < p_T < 10 \text{ GeV}/c, \quad |y| < 0.5 \quad (40)$$

STAR-2007

$$K^\pm : \quad \sqrt{S} = 200 \text{ GeV}, \quad 0.25 < p_T < 2.2 \text{ GeV}/c, \quad |y| < 0.5 \quad (41)$$

$$K_s^0 : \quad \sqrt{S} = 200 \text{ GeV}, \quad 0.26 < p_T < 4.7 \text{ GeV}/c, \quad |y| < 0.5 \quad (42)$$

STAR-2012, π^\pm, K^\pm, K_s^0 :

$$\sqrt{S} = 200 \text{ GeV}, \quad 3.0 < p_T < 15 \text{ GeV}/c, \quad |y| < 0.5 \quad (43)$$

The STAR Collaborations present their results for the hadronic yield $d^2N/dp_T dy$, extracted from the measured non-single diffractive (NSD) $p + p$ cross section, while our formulae are for the differential cross sections $d\sigma^h/d^3P_h$. The relation between them reads:

$$\sigma_{NSD} \frac{d^2N}{(2\pi) p_T dp_T dy} = E_h \frac{d\sigma_{pp}^h}{d^3P_h}(p_T, \theta(y)) \quad (44)$$

where σ_{NSD} is the measured total NSD $p + p$ cross section ($\sigma_{NSD} = 30.0 \pm 3.5$ mb) and $E_h d\sigma_{pp}^h/(d^3P_h)$ is our formula for the corresponding cross section – Eqs. (3), (29), (31) or (39).

In high energy hadron collider physics for the particle with the negligible mass the rapidity y coincides with the pseudo-rapidity η :

$$y \approx \eta \equiv \frac{1}{2} \ln \frac{1 + \cos \theta}{1 - \cos \theta} = -\ln \tan \frac{\theta}{2}, \quad (45)$$

and hence

$$\theta = 2 \arctan(e^{-\eta}) \approx 2 \arctan(e^{-y}). \quad (46)$$

As data from the STAR collaboration is presented averaged over rapidity: $|y| < 0.5$, which corresponds to $\theta \approx [\pi/3; \pi/2]$, we compare data to the following averaged over y expressions:

$$\sigma_{NSD} \frac{d^2N}{(2\pi) p_T dp_T dy} \Big|_{|y| < 0.5} = \int_{-0.5}^{0.5} dy E_h \frac{d\sigma_{pp}^h}{d^3P_h}(p_T, \theta(y)). \quad (47)$$

A. Results for charged pions

We calculate the p_T spectra of π^\pm using the parametrizations for $D_i^{\pi^\pm}$ obtained in HKNS-07, AKK-08, DSEHS-14 and LSS-15, and compare it to data on π^\pm -spectra measured by the STAR Collaborations STAR-2006 and STAR-2012 at $\sqrt{S} = 200$ GeV for different ranges of p_T and rapidity $|y| < 0.5$ – see Eqs. (40) and (43). All parametrizations are obtained within the same theoretical framework – NLO in QCD, assuming that isospin SU(2) symmetry of the u and d quarks for the favored and unfavored fragmentation functions holds at the initial scale Q_0^2 :

$$D_u^{\pi^+} = D_d^{\pi^+}, \quad D_{\bar{u}}^{\pi^+} = D_{\bar{d}}^{\pi^+} = D_s^{\pi^+} = D_{\bar{s}}^{\pi^+}. \quad (48)$$

Using charge conjugation invariance of strong interactions we have, in total, 3 independent FFs:

$$D_u^{\pi^+}, \quad D_d^{\pi^+}, \quad D_g^{\pi^+}. \quad (49)$$

The obtained FFs differ by the used data and the used parametrizations at Q_0^2 . Bellow we give the main sources of data of the used here FFs.

- In HKNS-07 the parametrizations and their uncertainties are obtained both in LO and NLO from analysis of the data on $e^+e^- \rightarrow \pi^\pm + X$. We use the NLO parameters and show the error band based on the Hessian method [27] and the error matrix provided by HKNS [4]. The analysis for kaons proceeds in the same manner.
- In AKK-08 the parametrizations are obtained from analysis of the data on $e^+e^- \rightarrow \pi^\pm + X$ and $pp \rightarrow \pi^\pm + X$.
- In DSEHS-14 the parametrizations are obtained in a global analysis of the data on $e^+e^- \rightarrow \pi^\pm + X$, $l+N \rightarrow \pi^\pm + X$ and $pp \rightarrow \pi^\pm + X$ including the STAR-2012 data. The uncertainties estimated within the Hessian approach are presented as shaded areas in their figures and the error matrix can be provided upon request. In turn, in our analysis, both for pions and kaons, we estimate the scale uncertainty when Q varies in the range $p_T/2 \leq Q \leq 2p_T$.
- In LSS-15 the parametrizations are obtained using the published HERMES data from 2013 on pion multiplicities from SIDIS $l + N \rightarrow \pi^\pm + X$ on proton and deuteron targets.

The results of our comparison to pion production are shown in Figs. 1–5 and in Table I. All p_T spectra for pions (and kaons in the next section) at the high energy $\sqrt{S} = 200$ GeV are presented for $p_T \geq 1$ GeV/c suitable for the perturbative QCD approach. This is consistent with the constraint on the $z_{min} = 0.01$, and $\min p_T = z_{min}\sqrt{S}/2$.

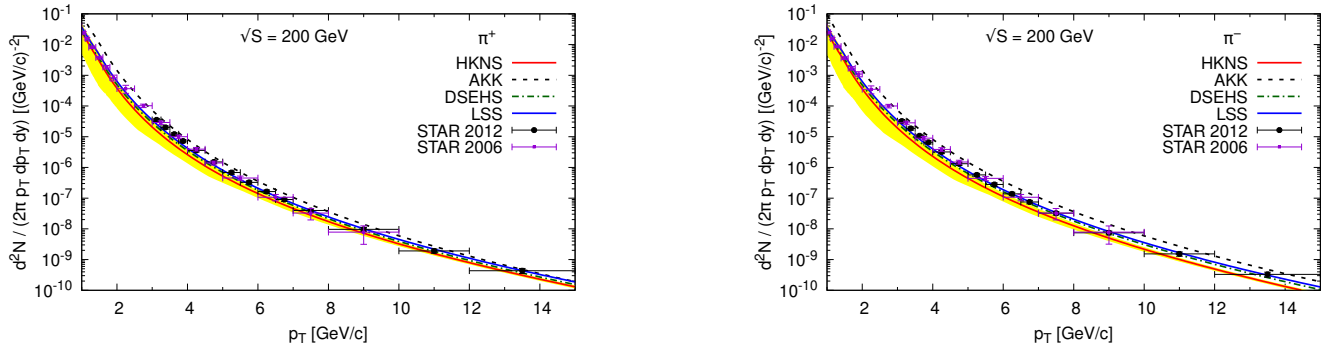


FIG. 1. The cross sections $\sigma_{pp}^{\pi^+}$ (left) and $\sigma_{pp}^{\pi^-}$ (right) calculated for different sets of FFs, compared to STAR-2006 and STAR-2012 data. The one- σ uncertainty band for HKNS FFs estimated by the Hessian method is shown.

In Figs. 1–3, we show the agreement of the p_T -spectra for the charged pions $\sigma_{pp}^{\pi^\pm}$ calculated for the different sets of FFs with the STAR-2006 and STAR-2012 data.

TABLE I. Values of χ^2 , Eq. (50), calculated for the single and difference cross sections in the pion production obtained for different FFs parametrizations.

FFs	π^+	π^-	$\pi^+ - \pi^-$
HKNS	10.2	11.7	0.136
AKK	77.2	83.3	-
DSEHS	4.55	4.39	0.148
LSS	2.83	2.46	0.143

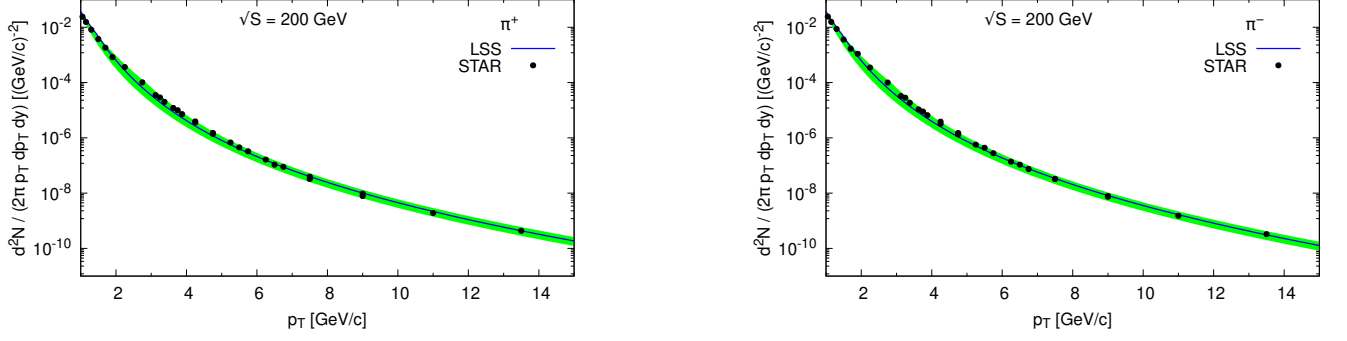


FIG. 2. The best fit LSS together with $\sigma_{pp}^{\pi^+}$ (left) and $\sigma_{pp}^{\pi^-}$ (right) STAR data. The theoretical uncertainties bands indicate the scale Q variation in the range $p_T/2 \leq Q \leq 2p_T$.

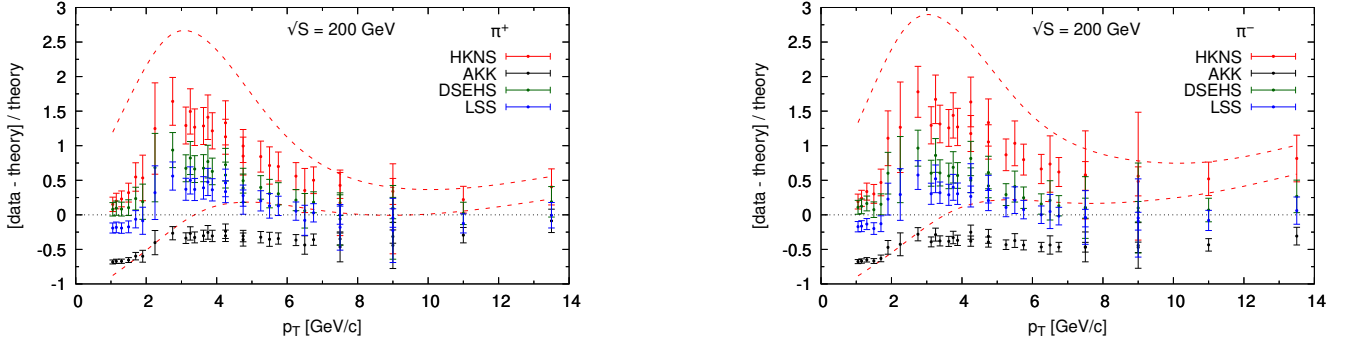


FIG. 3. The ratio (data-theory)/theory for the cross sections: $\sigma_{pp}^{\pi^+}$ (left) and $\sigma_{pp}^{\pi^-}$ (right) for different FFs. The experimental error bars and theoretical uncertainties for HKNS (dashed) are shown.

Using the values of χ^2 defined as

$$\chi^2 = \frac{1}{N} \sum_i^N \frac{(\sigma_i^{exp} - \sigma_i^{th})^2}{\Delta_i^2}, \quad (50)$$

where Δ_i^2 incorporates both statistical and systematic experimental errors, we are able to determine the best fit to the data. In our analysis for the pions, we took into account the combined STAR data for $p_T > 1 \text{ GeV}^2$ with $N = 30$ experimental points (STAR 2006 and STAR 2012). We find that the NLO LSS results agree the best with the data and the DSEHS fit which is partially based on the STAR-2012 data is comparably good as LSS. In Table I, we collect the values of χ^2 , Eq. (50), for the single charged pions π^\pm and also for the difference $\pi^+ - \pi^-$ obtained with the use of HKNS, AKK, DSEHS and LSS sets of FFs.

Fig. 4 shows a comparison of the difference cross section $\sigma_{pp}^{\pi^+ - \pi^-}$ calculated for different sets of FFs with the STAR-2006 and STAR-2012 data. Since the experimental errors are relatively large, all FFs parametrizations are comparably good for this nonsinglet case. Finally, in Fig. 5, using LSS FFs, we compare NLO and LO results for $\sigma_{pp}^{\pi^+}$. The right panel shows the K factor, defined as

$$K = \frac{[d\sigma_{pp}^h]^{NLO}}{[d\sigma_{pp}^h]^{LO}}, \quad (51)$$

where NLO calculations include the full α_s^3 radiative NLO corrections presented by Aversa et. al. in 1988, [14], and LO stands for the LO Born terms. It is seen that NLO predictions provide a better match to the data than LO ones, and the NLO corrections are more essential in the small p_t range. The middle panel of Fig. 5 shows the scale dependence of $\sigma_{pp}^{\pi^+}$ at LO and NLO where the scale Q may vary from $p_T/2$ to $2p_T$. It is seen that the scale dependence is clearly smaller at NLO. The same occurs for the polarized cross section for π^0 production, [6].

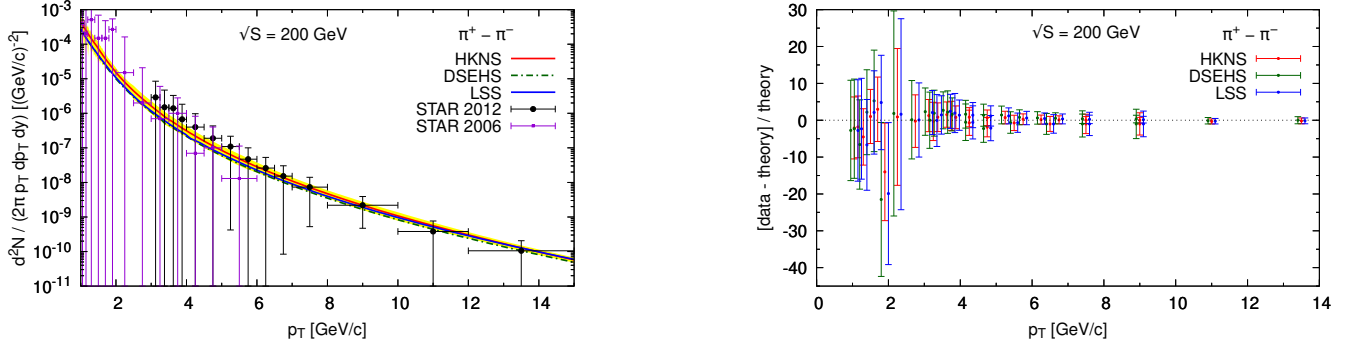


FIG. 4. Left: The difference cross section $\sigma_{pp}^{\pi^+\pi^-}$ calculated for different sets of FFs, compared to the STAR data. The one- σ uncertainty band for HKNS FFs is shown. Right: The ratio (data-theory)/theory for the difference cross section. The experimental error bars are shown. For better visibility points for DSEHS (LSS) are displaced by -0.1 (+0.1) in p_T .

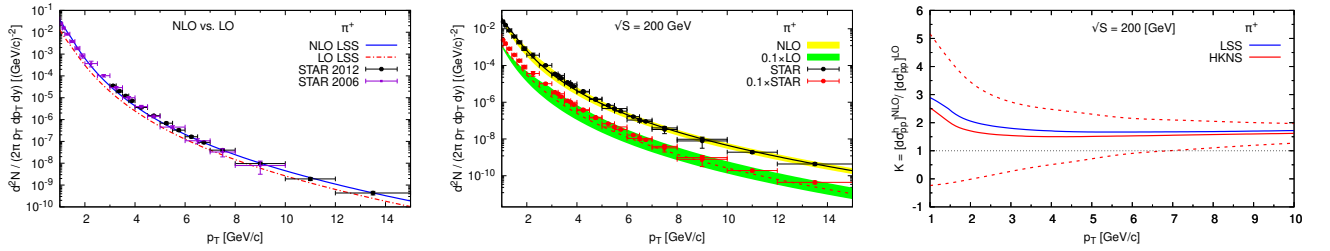


FIG. 5. Left: a comparison of the NLO and LO results for the cross section $\sigma_{pp}^{\pi^+}$ with the use of LSS FFs together with the STAR data. Middle: the scale dependence of $\sigma_{pp}^{\pi^+}$ at LO and NLO for LSS FFs. The shaded bands indicate the uncertainties from varying the Q scale in the range $p_T/2 \leq Q \leq 2p_T$. The solid (dashed) lines are for the choice $Q = p_T$. For better visibility, the LO results (and the STAR data, respectively) are rescaled by 0.1. Right: the K factor, Eq. (51), vs p_T for the HKNS and LSS results at the choice $Q = p_T$. The error band for HKNS is shown (dashed).

B. Results for charged kaons

We calculate the p_T spectra of K^+ using the parametrizations for $D_i^{K^+}$ obtained in HKNS-07, AKK-08 and DSEHS-17, and compare it to data on K^\pm -spectra measured by the STAR Collaborations STAR-2007 and STAR-2012 at $\sqrt{S} = 200$ GeV for different ranges of p_T and rapidity $-0.5 < y < 0.5$ – see Eqs. (41) and (43). All considered parametrizations of $D_q^{K^+}$ are obtained within the same theoretical framework – NLO in QCD¹, using the simplifying assumption that at the initial scale Q_0^2 all unfavored fragmentation functions are equal:

$$D_{\bar{u}}^{K^+}(z, Q_0^2) = D_d^{K^+}(z, Q_0^2) = D_s^{K^+}(z, Q_0^2) = D_g^{K^+}(z, Q_0^2). \quad (52)$$

If neutral kaons are considered then SU(2) invariance relates the FFs of K^0 to those for charged kaons and thus no new FFs are introduced, and, as shown, this leads to relation (39). If only charged kaons are involved there are no SU(2) constraints. SU(2) invariance enters the game only when K^0 are measured as well. Taking into account also charge conjugation invariance of strong interactions we end up, in total, with 4 independent kaon FFs:

$$D_u^{K^+}, \quad D_{\bar{u}}^{K^+}, \quad D_{\bar{s}}^{K^+}, \quad D_g^{K^+}. \quad (53)$$

Below we give the main characteristics of the FFs used here.

- In HKNS-07 the parametrizations are obtained both in LO and NLO in QCD from an analysis of the data on $e^+e^- \rightarrow K^\pm + X$. We use the NLO parameters.

¹ In an interesting study [28], Demirci and Ahmadov have considered various models of FFs and also the effect of HT in charged kaon production and suggested that HT effects may be large in certain kinematic regions.

- In AKK-08 the parametrizations are obtained in NLO from an analysis of the data on $e^+e^- \rightarrow K^\pm + X$ and $pp \rightarrow K^\pm + X$. No uncertainties of the obtained parametrizations are presented.
- In DSEHS-17 the parametrizations are obtained in a global analysis of the data on $e^+e^- \rightarrow K^\pm + X$, $l + N \rightarrow K^\pm + X$ and $pp \rightarrow K^\pm + X$ including the STAR-2012 data. The parameters of the FFs are presented in NLO, using the same assumption Eq. (52) that all unfavoured FFs at the initial scale Q_0^2 are the same, but here at NLO.

Our results for kaons are presented in Figs. 6–10 and in Table II in a similar way as those for pions.

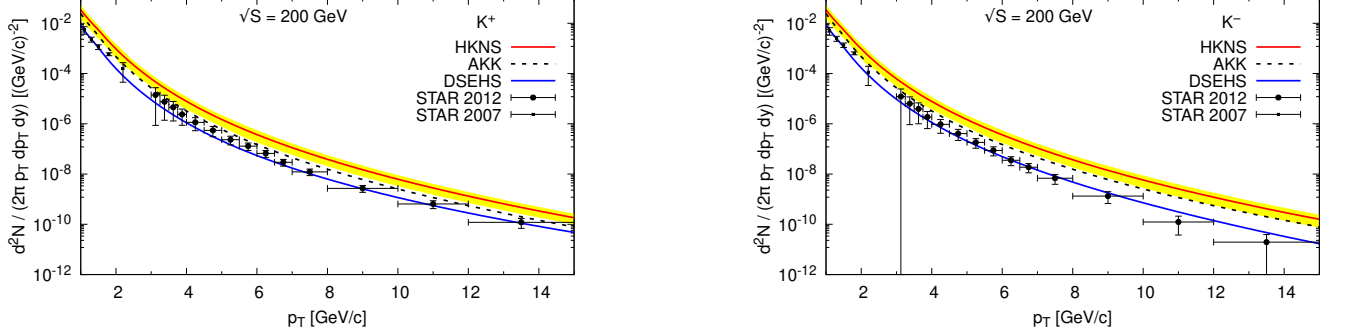


FIG. 6. The cross sections $\sigma_{pp}^{K^+}$ (left) and $\sigma_{pp}^{K^-}$ (right) calculated for different sets of FFs, compared to STAR-2007 and STAR-2012 data. The one- σ uncertainty band for HKNS FFs estimated by the Hessian method is shown.

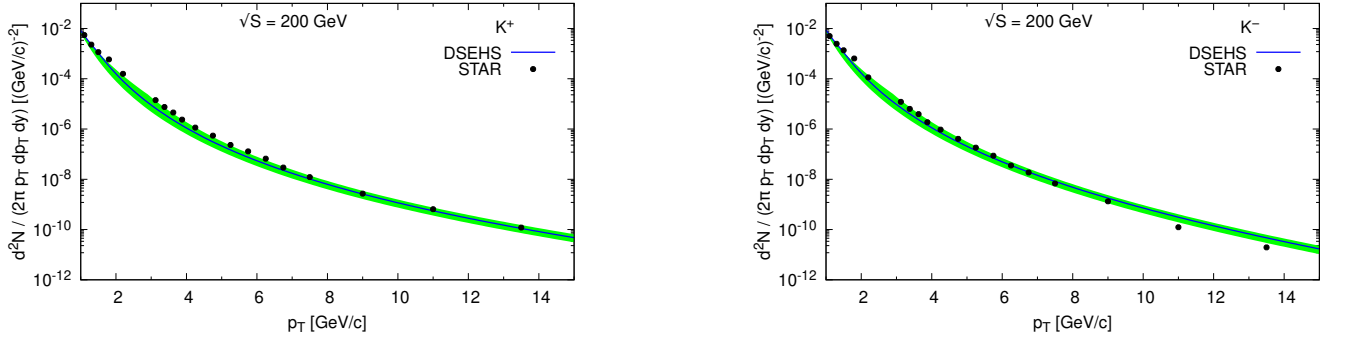


FIG. 7. The best fit DSEHS together with $\sigma_{pp}^{K^+}$ (left) and $\sigma_{pp}^{K^-}$ (right) STAR data. The theoretical uncertainties bands indicate the scale Q^2 variation in the range $p_T/2 \leq Q \leq 2p_T$.

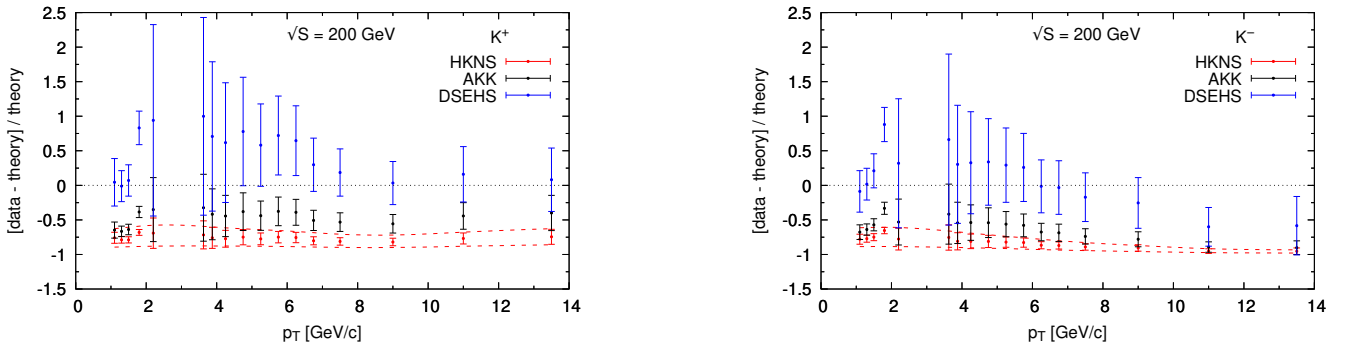


FIG. 8. The ratio (data-theory)/theory for the cross sections: $\sigma_{pp}^{K^+}$ (left) and $\sigma_{pp}^{K^-}$ (right) for different FFs. The experimental error bars and theoretical uncertainties for HKNS (dashed) are shown.

From Figs. 6–8 and also from the χ^2 analysis, Eq. (50), it is seen that the DSEHS-17 FFs which are based also on the STAR-2012 data provide the best fit. We took into account the combined STAR data for $p_T > 1 \text{ GeV}^2$ with

TABLE II. Values of χ^2 , Eq. (50), calculated for the single and difference cross sections in the kaon production obtained for different FFs parametrizations.

FFs	K^+	K^-	$K^+ - K^-$
HKNS	124	222	0.335
AKK	16.0	34.1	-
DSEHS	1.18	1.31	0.329

$N = 17$ experimental points (STAR 2007 and STAR 2012). In Table II, we collect the values of χ^2 , Eq. (50), for the single charged kaons K^\pm and also for the difference $K^+ - K^-$ obtained with the use of HKNS, AKK and DSEHS sets of FFs.

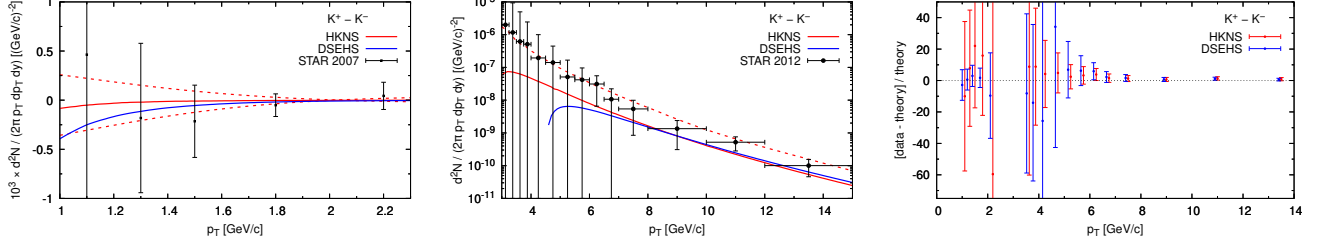


FIG. 9. The difference cross section $\sigma_{pp}^{K^+ - K^-}$ calculated for different sets of FFs, compared to the STAR data. Left: for the small p_T range. The one- σ uncertainty band for HKNS FFs is shown (dashed). Middle: for $p_T > 3$ GeV/c. Since the theoretical error for HKNS is larger than the value of $\sigma_{pp}^{K^+ - K^-}$ itself, we show only the upper line of the uncertainty (dashed). Right: The ratio (data-theory)/theory for the difference cross section. The experimental error bars are shown. For better visibility points for DSEHS are displaced by -0.1 in p_T .

A comparison of the difference cross section $\sigma_{pp}^{K^+ - K^-}$ obtained for different sets of FFs with the STAR-2007 and STAR-2012 data is presented in Fig. 9. For some experimental points of STAR-2007 and also for the theoretical predictions at $p_T < 3$ GeV/c for HKNS and $p_T < 4.5$ GeV/c for DSEHS $\sigma_{pp}^{K^+ - K^-} < 0$. Again, similarly as for pions, the large experimental errors make useless the idea to find the best fit.

A comparison of the NLO and LO predictions to the data for $\sigma_{pp}^{K^+}$ presented in Fig. 10 shows, similarly as in the pion case, better agreement of the NLO results with the data. From the middle panel one can see the smaller scale dependence at NLO. The K factor, Eq. (51), obtained for $Q = p_T$, presented in the right panel of Fig. 10, varies between about 2 for $p_T = 10$ GeV/c to 3 for $p_T = 1$ GeV/c.

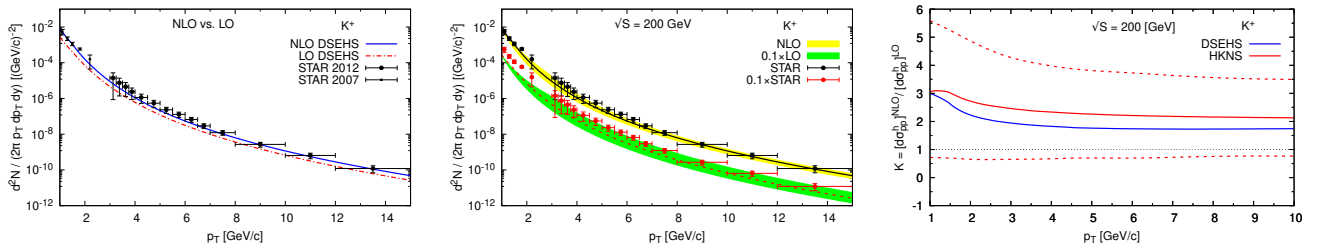


FIG. 10. Left: a comparison of the NLO and LO results for the cross section $\sigma_{pp}^{K^+}$ with the use of DSEHS FFs together with the STAR data. Middle: the scale dependence of $\sigma_{pp}^{K^+}$ at LO and NLO for DSEHS FFs. The shaded bands indicate the uncertainties from varying the Q scale in the range $p_T/2 \leq Q \leq 2p_T$. The solid (dashed) lines are for the choice $Q = p_T$. For better visibility, the LO results (and the STAR data, respectively) are rescaled by 0.1. Right: the K factor, Eq. (51), vs p_T for the HKNS and DSEHS results at the choice $Q = p_T$. The error band for HKNS is shown (dashed).

C. Results for neutral and charged kaons $K^+ + K^- - 2K_s^0$

It is important to recall that if not only charged, but neutral kaons are measured, as well, and if SU(2) isospin symmetry holds no new kaon FFs are introduced. In this section, we shall test SU(2) invariance of the u and d quarks

for kaons.

If the FFs of both charged and neutral kaons are extracted independently from the data, then they should satisfy Eq. (32). Only in AKK [5] the neutral and charged kaons FFs are obtained separately, without imposing SU(2)-invariance. This allows to test Eq. (32) and study the SU(2)- symmetry directly.

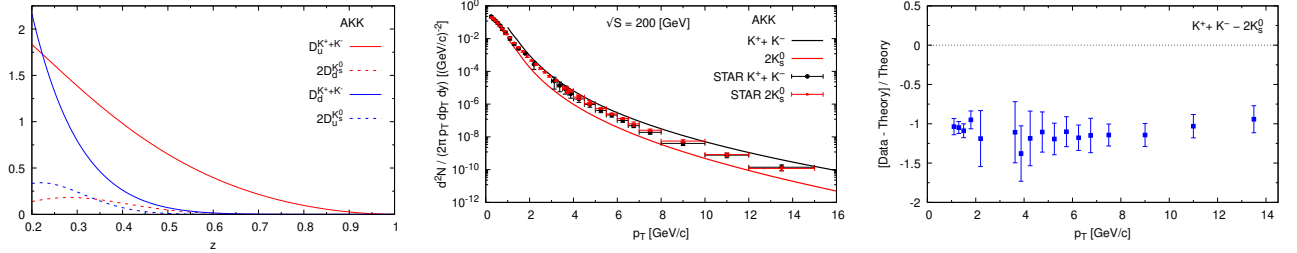


FIG. 11. Left: Test of the SU(2) invariance via Eq. (32) for AKK FFs. Middle: A comparison of the AKK predictions with the STAR data for $K^+ + K^-$ and $2K_s^0$. Right: $[Data - Theory]/Theory$ for $K^+ + K^- - 2K_s^0$. The experimental error bars are shown.

In the left panel of Fig. 11, we compare $D_u^{K^+K^-}$ with $2D_d^{K_s^0}$ and $D_d^{K^+K^-}$ with $2D_u^{K_s^0}$. This clearly shows that isospin symmetry is badly broken for the AKK-08 kaon FFs. It is also visible in the middle and right panels of the same figure. The experimental STAR data for kaons where $\sigma^{K^+K^-} = \sigma^{2K_s^0}$ confirm the SU(2)-invariance. The theoretical predictions for HKNS and DSEHS based on FFs for which the SU(2)-invariance is assumed also provides, contrary to AKK, $\sigma^{K^+K^-} - \sigma^{2K_s^0} = 0$.

In summary, the above studies clearly show that one can distinguish two types of parametrizations of the FFs that describe the p_T -spectra of the produced charged kaons in pp collisions: HKNS and DSEHS, for which SU(2)-invariance holds - that agrees with the data - and AKK for which it does not. For this reason, making the predictions for NICA, we shall not longer consider AKK a reasonable fit for kaons.

V. RESULTS FOR NICA PROJECT – PIONS AND KAONS

NICA (Nuclotron-based Ion Collider fAcility) is a new accelerator complex under construction at the Joint Institute for Nuclear Research in Dubna. In anticipation of the NICA results we have produced estimates of various semi-inclusive cross-sections based on the discussed above FFs. These should be useful for planning experiments.

The accelerated beams in NICA by design will consist of particles ranging from protons and light nuclei to fully stripped gold ions. Beam energies for $p + p$ collisions will span $\sqrt{S} = 12 - 27$ GeV with luminosity $L_{pp} \geq 10^{30} \text{ cm}^{-2} \text{ s}^{-1}$, and $\sqrt{S_{NN}} = 4 - 11$ GeV with averaged luminosity $L_{Au+Au} = 10^{27} \text{ cm}^{-2} \text{ s}^{-1}$ for heavy-ion $Au + Au$ collisions [23, 24]. The expected ranges of p_T and pseudo-rapidity η , Eq. (45), in NICA Multi Purpose Detector (MPD) for identification of pions and kaons are:

$$0.1 \text{ GeV}/c < p_T < 2 \text{ GeV}/c \quad (54)$$

$$0.1 \pi < \theta < 0.9 \pi \rightarrow |\eta| < 2, \quad (55)$$

providing almost the whole forward hemisphere in which the final hadrons will be detected.

Below, we present the NLO pQCD predictions for NICA energies and p_T based on the viable sets of FFs elaborated in the previous sections. We find it interesting to compare them with the existing data from the STAR experiment in the Beam Energy Scan (BES) program at the Relativistic Heavy Ion Collider (RHIC) on the hadron production in Au+Au collisions at the energies similar to those planned at NICA [29].

We use the phenomenological result that spectral shapes and relative particle yields are similar in $p + p$ and peripheral $A + A$ collisions where the nuclear effects are negligible [21, 22]. Thus, one can regard the nuclei as an incoherent superposition of partons and approximate the A+A collisions as a sum of independent nucleon-nucleon (N+N) collisions. In this approach, the hard process inclusive yield in nuclear collisions is expected to scale as N_{coll} , the average number of inelastic N+N collisions [21, 22], and the nuclear modification factor is defined as a ratio:

$$R_{AA}(p_T) = \frac{d^2 N^{AA} / dp_T dy}{N_{\text{coll}} d^2 N^{NN} / dp_T dy}. \quad (56)$$

In the absence of nuclear modifications to hard scattering, $R_{AA} = 1$, and we obtain the scaling relation between inclusive yields in $p + p$ and peripheral ($R_{AA} = 1$) $A + A$ collisions:

$$\frac{d^2 N^{AA}}{dp_T dy} = N_{\text{coll}} \frac{d^2 N^{pp}}{dp_T dy}, \quad (57)$$

where

$$\frac{d^2 N^{pp}}{2\pi p_T dp_T dy} = \frac{1}{\sigma_{inel}^{pp}} E_h \frac{d\sigma_{pp}^h}{d^3 P_h}. \quad (58)$$

In the first step, we illustrate the scaling, Eqs. (57) and (58) at high energy $\sqrt{S} = 200$ GeV by comparing our NLO pQCD results for p_T spectra of π^+ in $p + p$ collisions with the STAR data on the semi-inclusive hadron production in the most peripheral Au+Au collisions [30]. We used the best fit, i.e., LSS parametrization of FFs. For thus chosen the most peripheral events, nuclear corrections can be neglected, and the scaling works, i.e., the pQCD results for $p + p$ scaled up, according to Eqs. (57) and (58), by $N_{\text{coll}}/\sigma_{inel}^{pp}$, where N_{coll} is provided with the experimental data, give the results for Au+Au (most peripheral). This is shown in Fig. 12 where we plot Au+Au data [30] for the most peripheral collisions (centrality 60 – 80%)² and also NSD $p + p$ data [15–17].

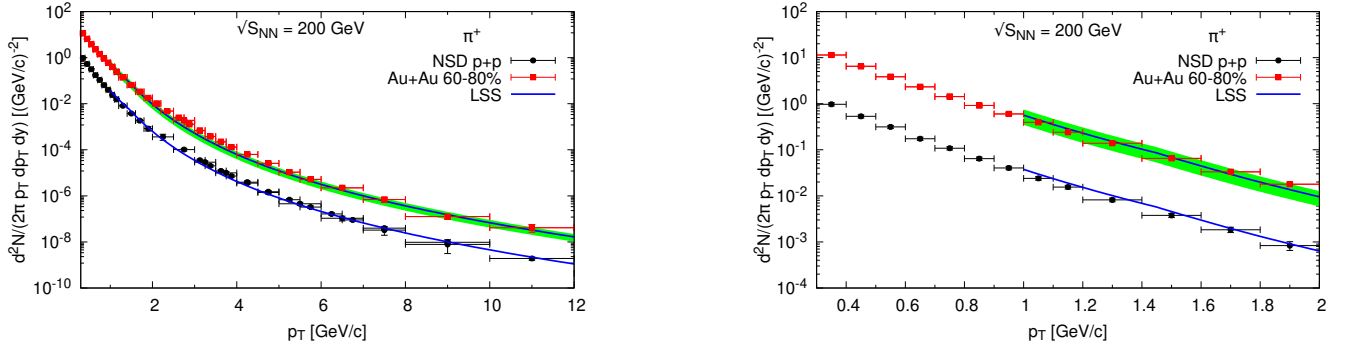


FIG. 12. Transverse momentum spectra for π^+ in $p + p$ and Au+Au the most peripheral collisions (centrality 60 – 80%) at $\sqrt{S} = 200$ GeV and midrapidity $|y| < 0.5$. NLO pQCD reference for LSS parametrization of FFs is scaled up for Au+Au by $N_{\text{coll}} = 21.2^{+6.6}_{-7.9}$, Eqs. (57) and (58), where $\sigma_{inel}^{pp} = 42$ mb for $\sqrt{S} = 200$ GeV [32]. The error bands correspond to the systematic uncertainties of N_{coll} . Right panel: same as in the left panel but for NICA kinematics of $p_T < 2$ GeV/c.

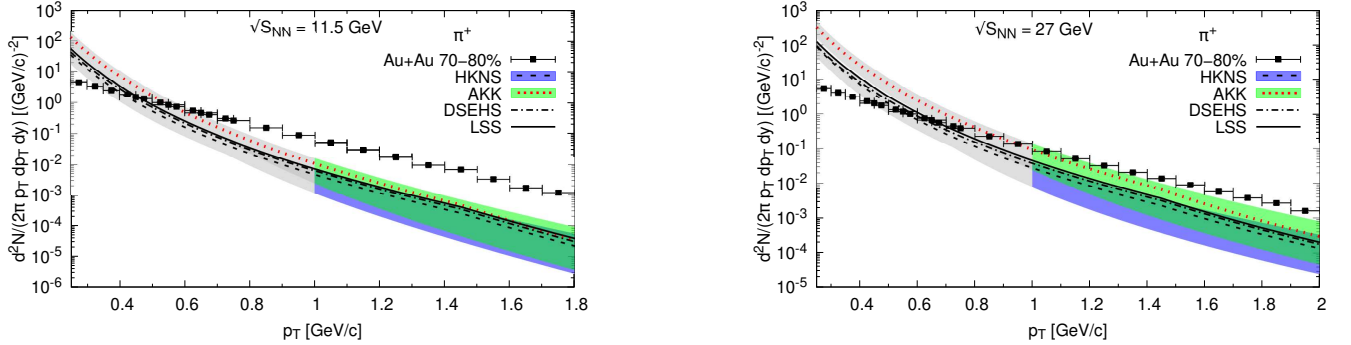


FIG. 13. Transverse momentum spectra for π^+ in Au+Au the most peripheral collisions (centrality 70–80%) at $\sqrt{S} = 11.5$ GeV (left) and $\sqrt{S} = 27$ GeV (right), and midrapidity $|y| < 0.1$, [29]. NLO pQCD references for different FFs parametrizations are scaled up by $N_{\text{coll}} = 14 \pm 7$, Eqs. (57) and (58), where $\sigma_{inel}^{pp} = 33$ mb for $\sqrt{S} = 27$ GeV and 31 mb for $\sqrt{S} = 11.5$ GeV [32]. The error bands, which for better visibility are shown only for AKK and HKNS fits, correspond to the systematic uncertainties of N_{coll} and theoretical uncertainties due to Q scale variation, $p_T/2 \leq Q \leq 2p_T$. Gray bands correspond to the non-perturbative $p_T < 1$ GeV/c region where the pQCD analysis may be insufficient.

² Details on centralities and N_{coll} values estimations using a Glauber model can be found in [31].

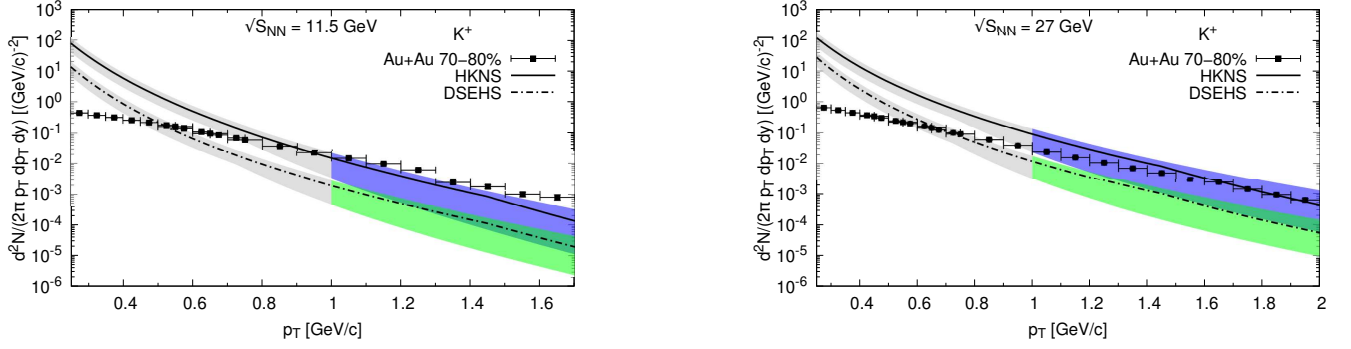
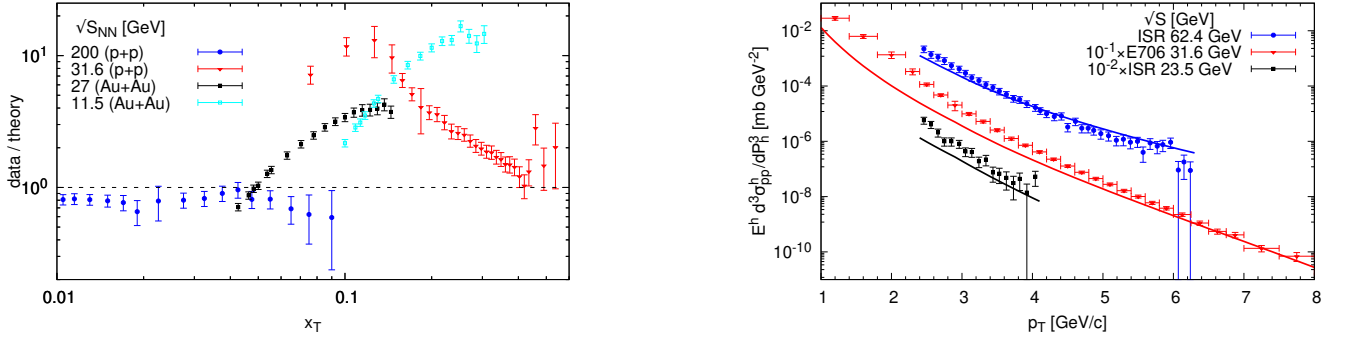
FIG. 14. Same as in Fig. 13 but for K^+ .

FIG. 15. Left: ratios of data to theory for the inclusive π^+ (STAR), and also π^0 (E706), production in $p + p$ and the most peripheral Au+Au collisions as a function of x_T at different $\sqrt{S_{NN}}$: 200, 27 and 11.5 GeV at STAR, and 31.6 GeV at E706. Right: the NLO pQCD results for the p_T spectra of π^0 at different \sqrt{S} compared to the measurements in $p + p$ collisions at ISR and E706.

One can expect a similarly good scaling behaviour of the p_T spectra for pions and kaons also at NICA kinematics. Figs. 13 and 14 present our results for π^+ and K^+ based on different FFs fits compared with the STAR data on Au+Au most peripheral collisions at centrality 70 – 80% and c.m. energies $\sqrt{S} = 11.5$ and 27 GeV [29]. In our analysis for low energies and low $p_T < 1$ GeV/c, we freeze QCD evolution of PDFs and FFs at the scale $Q_0^2 = 1$ GeV². Nevertheless, the pQCD predictions without non-perturbative transverse momentum corrections (e.g. higher-twist effects in PDFs and FFs), which still are not under theoretical control, makes this analysis insufficient. Therefore, we draw attention mostly to our predictions for NICA obtained for $1 < p_T < 2$ GeV/c.

In turn, for $p_T > 1$ GeV/c, one sees from Figs. 13 and 14 that the NLO pQCD results for LSS and DSEHS FFs, which provide the best fits to the STAR data at $\sqrt{S} = 200$ GeV, here, for much lower energy, predict yields that are significantly below the data at low p_T . Such discrepancies have been observed or expected in all hard processes and interpreted as an impact of an additional soft-gluon emission at the initial state [33, 34]. This effect causes sizable parton k_T which is not taken into account in the NLO pQCD calculation.

Deviations between measured inclusive pion cross sections and NLO pQCD calculations are visible mostly for $x_T = 2p_T/\sqrt{S} \gtrsim 0.1$ [33]. This is illustrated in Fig. 15 (left), where we plot ratios of data to theory for the inclusive pion production in $p + p$ and the most peripheral Au + Au collisions as a function of x_T at different $\sqrt{S_{NN}}$. In the right panel, we compare the p_T spectra for pions at different \sqrt{S} to the measurements in $p + p$ collisions. We use the LSS theoretical predictions and the experimental data on π^+ , and also π^0 , at the energy scales from 11.5 up to 200 GeV [15–17, 29, 30, 34, 35]. It's seen that discrepancies between data and theory grow with decreasing energy and become significant at about $\sqrt{S} = 60$ GeV. Thus, scaling, Eqs. (57) and (58), works well at high energies, significantly above the energy scales specific for NICA.

Finally, let us discuss different behaviour of the antiparticle to particle ratios of the p_T spectra at the lower BES energies in comparison to those at $\sqrt{S} = 200$ GeV. It could be a key to distinguish between various FFs parametrizations.

The experimental results from Au+Au collisions at $\sqrt{S_{NN}} = 11.5$ and 27 GeV show that the π^-/π^+ ratio is mostly

positive and close to unity in contrast to our theoretical prediction, and also to the data at $\sqrt{S} = 200$ GeV, where $\pi^+ > \pi^-$, see Fig. (16). In turn, the ratio for kaons, K^-/K^+ , exhibit an interesting trend, namely, it increases with increasing energy and lies significantly below unity at the lower BES energies, see Fig. (17). This reflects the increasing contribution to K^- production via pair production which dominates over so called associated production at higher energies (e.g. $NN \rightarrow KYN$, where Y denotes a hyperon). These behaviours of π^-/π^+ and K^-/K^+ ratios are very little centrality dependent and occur also for the peripheral collisions under study.

It is reasonable to assume that at a given energy the additional initial state soft-gluon emission corrections are the same for particles and antiparticles produced in $p + p$ collisions. Therefore, these corrections, which are not included in the NLO pQCD analysis, can possibly be neglected when we study the ratio of the p_T spectra, h^-/h^+ . In the light of this assumption, one can see from Figs. (16) and (17) that while the data do not agree with theory there is some preference for the LSS-15 and DSEHS-14 FFs for pions and DSEHS-17 for kaons over the HKNS one.

For the difference cross sections, $\sigma_{pp}^{h^+-h^-}$, the gap between predictions for different FFs is undetectably small within the theoretical uncertainty bands, see Fig. (18), and the measurements of $\sigma^{h^+-h^-}$ cannot distinguish between various FFs sets.

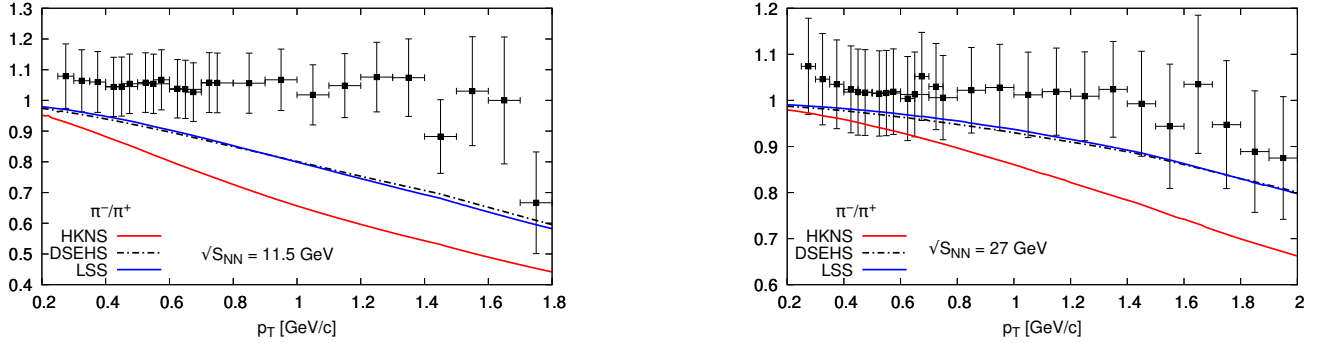


FIG. 16. The ratios of the p_T spectra for π^-/π^+ in Au+Au the most peripheral collisions at $\sqrt{S} = 11.5$ GeV (left) and $\sqrt{S} = 27$ GeV (right) compared with the NLO pQCD results.

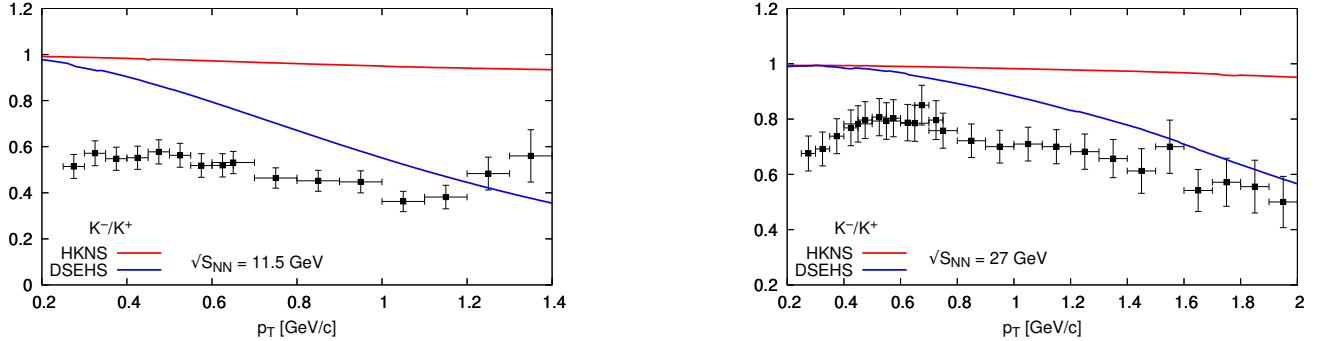


FIG. 17. Same as in Fig. 16 but for kaons.

CONCLUSIONS

There exist in the literature several different relatively up to date expressions for the pion and kaon fragmentation functions: HKNS-07 [4], AKK-08 [5], DSEHS-14 [1], DSEHS-17 [2] and LSS-15 [3] and we have attempted, in this paper, to examine which, if any, of these is compatible with the STAR data on semi-inclusive pion and kaon production in proton-proton collisions. We have thus compared the predictions for the semi-inclusive cross-sections $pp \rightarrow \text{pions} + X$ and $pp \rightarrow \text{kaons} + X$ based on these FFs with the data from the STAR collaboration. Of the published FFs all except AKK respect isospin invariance. As seen in Fig. 11, AKK fails badly to describe the data on $pp \rightarrow K^+ + K^- - 2K_s^0$,

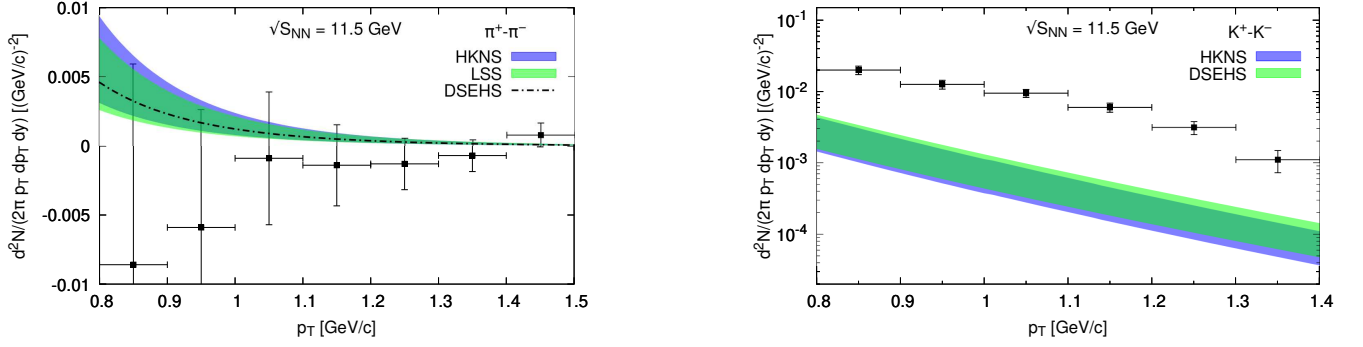


FIG. 18. The p_T spectra of the difference cross sections, $\pi^+ - \pi^-$ (left), and $K^+ - K^-$ (right) in Au+Au the most peripheral collisions at $\sqrt{S} = 11.5$ GeV compared with the NLO pQCD results for different FFs.

so is no longer considered a viable FF for kaons. All the others provide a good fit to the STAR data, with both LSS-15 and DSEHS-14 for pions and DSEHS-17 for kaons significantly better than the others.

Furthermore, we have compared the results for the cross sections obtained within LO and NLO approaches and studied their scale- Q^2 dependence, where Q may vary from $p_T/2$ to $2p_T$. We found that the NLO predictions fit clearly better the data, specially in the small p_T range, and are less scale dependent than the LO ones.

In our paper, we have also obtained estimates of various semi-inclusive cross-sections based on the above viable FFs for the future run of the NICA accelerator. This is achieved comparing our NLO pQCD results with the existing data from the STAR experiment in the BES program at RHIC on the hadron production in the most peripheral Au+Au collisions, where the nuclear effects are negligible, at the energies similar to those planned at NICA [29]. Disagreement between data and theory at $\sqrt{S} = 11.5$ and 27 GeV shows that a purely pQCD approach is inadequate and suggests the necessity to take into account also higher-order effects of initial-state soft-gluon radiation, [33, 34], not included in the NLO pQCD approach. Nevertheless, these data on the p_T spectra of π^+ , K^+ and also the ratios π^-/π^+ and K^-/K^+ , (see Figs. 13, 14 and 16, 17) seem favour LSS-15 and DSEHS-14 FFs for pions and DSEHS-17 for kaons, similarly as at the energy scale $\sqrt{S} = 200$ GeV. We have also check that the measurements of the difference cross sections, $\sigma^{h^+ - h^-}$, cannot distinguish between various FFs sets (see Fig. 18).

ACKNOWLEDGEMENTS

E.C. and D.K. acknowledge the support of the INRNE-BAS (Bulgaria) - JINR (Russia) collaborative Grant, E.C. – of Grant KP-06-N58/5 of the Bulgarian Science Foundation and D.K. – of the Bogoliubov-Infeld Program. D.K. is grateful to S.V. Mikhailov and A. Kotlorz for useful discussions on numerical analysis.

Appendix A: The partonic subprocesses contributing to $pp \rightarrow hX$

Following the paper [9], we obtain the expression for the inclusive cross section $pp \rightarrow hX$:

$$E^h \frac{d\sigma_{pp}^h}{d^3P^h} = \frac{1}{\pi} \sum_{ab \rightarrow cd} \int_{x_{a,min}}^1 dx_a \int_{x_{b,min}}^1 dx_b \frac{1}{z} q_a(x_a) q_b(x_b) \frac{d\hat{\sigma}_{ab}^{cd}}{dt} D_c^h(z). \quad (A1)$$

where

$$s = x_a x_b S, \quad t = \frac{x_a}{z} T, \quad u = \frac{x_b}{z} U, \quad z = -\frac{x_a T + x_b U}{x_a x_b S} \quad (A2)$$

The lower limits of integration are determined by the conditions $z < 1$ and $s + t + u = 0$ [9]:

$$x_{a,min} = \frac{-U}{T + S} \quad (A3)$$

$$x_{b,min} = \frac{-x_a T}{x_a S + U} \quad (A4)$$

Hence, we can calculate the contributions from the different partonic subprocesses of Eq. (A1),

$$q_a(x_a)q_b(x_b) \frac{d\hat{\sigma}_{ab}^{cd}}{dt} D_c^h(z). \quad (\text{A5})$$

Below, we give formulas for all possible $ab \rightarrow cd$ contributions together with detailed examples.

The general formula is:

$$q_a(x_a)q_b(x_b) \left[\frac{d\hat{\sigma}_{ab}^{cd}}{dt} D_c^h(z) + \frac{d\hat{\sigma}_{ab}^{cd}}{du} D_d^h(z) \right] + q_a(x_b)q_b(x_a) \left[\frac{d\hat{\sigma}_{ab}^{cd}}{du} D_c^h(z) + \frac{d\hat{\sigma}_{ab}^{cd}}{dt} D_d^h(z) \right], \quad (\text{A6})$$

where

$$1. \hat{\sigma}_1: q_i q_j \rightarrow q_i q_j, \quad \bar{q}_i \bar{q}_j \rightarrow \bar{q}_i \bar{q}_j, \quad q_i \bar{q}_j \rightarrow q_i \bar{q}_j, \quad \bar{q}_i q_j \rightarrow \bar{q}_i q_j, \quad i \neq j$$

$$\begin{aligned} \hat{\sigma}_1 : & \sum_{i \neq j} q_i(x_a)q_j(x_b) \left[D_{q_i}^h \frac{d\hat{\sigma}_1}{dt} + D_{q_j}^h \frac{d\hat{\sigma}_1}{du} \right] + \bar{q}_i(x_a)\bar{q}_j(x_b) \left[D_{\bar{q}_i}^h \frac{d\hat{\sigma}_1}{dt} + D_{\bar{q}_j}^h \frac{d\hat{\sigma}_1}{du} \right] \\ & + q_i(x_a)\bar{q}_j(x_b) \left[D_{q_i}^h \frac{d\hat{\sigma}_1}{dt} + D_{\bar{q}_j}^h \frac{d\hat{\sigma}_1}{du} \right] + \bar{q}_i(x_a)q_j(x_b) \left[D_{\bar{q}_i}^h \frac{d\hat{\sigma}_1}{dt} + D_{q_j}^h \frac{d\hat{\sigma}_1}{du} \right] \\ = & \sum_{i \neq j} [q_i(x_a)D_{q_i}^h + \bar{q}_i(x_a)D_{\bar{q}_i}^h] \tilde{q}_j(x_b) \frac{d\hat{\sigma}_1}{dt} + [q_j(x_b)D_{q_j}^h + \bar{q}_j(x_b)D_{\bar{q}_j}^h] \tilde{q}_i(x_a) \frac{d\hat{\sigma}_1}{du} \\ & i \neq j : i = u, j = d, s; \quad i = d, j = u, s, \quad i = s, j = u, d. \end{aligned} \quad (\text{A7})$$

$$\begin{aligned} \sigma_1^{h-\bar{h}} : & \sum_{i \neq j} \left\{ q_{iV}(x_a) \tilde{q}_j(x_b) D_{q_{iV}}^h \frac{d\hat{\sigma}_1}{dt} + q_{jV}(x_b) \tilde{q}_i(x_a) D_{q_{jV}}^h \frac{d\hat{\sigma}_1}{du} \right\}, \\ & i \neq j : i = u, j = d, s; \quad i = d, j = u, s, \quad i = s, j = u, d. \end{aligned} \quad (\text{A8})$$

$$\begin{aligned} \sigma_1^{h+\bar{h}} : & = \sum_{i \neq j} \left[\tilde{q}_i(x_a) \tilde{q}_j(x_b) D_{q_i}^{h+\bar{h}} \frac{d\hat{\sigma}_1}{dt} + \tilde{q}_j(x_b) \tilde{q}_i(x_a) D_{q_j}^{h+\bar{h}} \frac{d\hat{\sigma}_1}{du} \right] \\ & i \neq j : i = u, j = d, s; \quad i = d, j = u, s, \quad i = s, j = u, d. \end{aligned} \quad (\text{A9})$$

$$2. \hat{\sigma}_2: q_i q_i \rightarrow q_i q_i, \quad \bar{q}_i \bar{q}_i \rightarrow \bar{q}_i \bar{q}_i$$

$$\hat{\sigma}_2 : \sum_{i=u,d,s} [q_i(x_a)q_i(x_b) D_{q_i}^h(z) + \bar{q}_i(x_a)\bar{q}_i(x_b) D_{\bar{q}_i}^h(z)] \frac{d\hat{\sigma}_2}{dt}, \quad (\text{A10})$$

symmetric in $t - u$.

$$\begin{aligned} \hat{\sigma}_2^{h-\bar{h}} : & \sum_{q=u,d,s} [q(x_a)q(x_b) - \bar{q}(x_a)\bar{q}(x_b)] D_{qV}^h(z) \frac{d\hat{\sigma}_2}{dt} \\ = & \sum_{q=u,d,s} \frac{1}{2} [q_V(x_a)\tilde{q}(x_b) + \tilde{q}(x_a)q_V(x_b)] D_{qV}^h(z) \frac{d\hat{\sigma}_2}{dt}. \end{aligned} \quad (\text{A11})$$

$$\hat{\sigma}_2^{h+\bar{h}} : \sum_{q=u,d,s} [q(x_a)q(x_b) + \bar{q}(x_a)\bar{q}(x_b)] \frac{d\hat{\sigma}_2}{dt} D_q^{h+\bar{h}}(z). \quad (\text{A12})$$

$$3. \hat{\sigma}_3: q_i \bar{q}_i \rightarrow q_j \bar{q}_j, \quad i \neq j$$

$$\hat{\sigma}_3 : \sum_{i \neq j} [q_i(x_a)\bar{q}_i(x_b) + \bar{q}_i(x_a)q_i(x_b)] \frac{d\hat{\sigma}_3}{dt} D_{j+\bar{j}}^h(z). \quad (\text{A13})$$

symmetric in $t - u$.

$$\hat{\sigma}_3^{h+\bar{h}} : \sum_{i \neq j} 2 [q_i(x_a)\bar{q}_i(x_b) + \bar{q}_i(x_a)q_i(x_b)] \frac{d\hat{\sigma}_3}{dt} D_j^{h+\bar{h}}(z). \quad (\text{A14})$$

4. $\hat{\sigma}_4: q_i \bar{q}_i \rightarrow q_i \bar{q}_i$:

$$\hat{\sigma}_4 : \quad \sum_i \left\{ q_i(x_a) \bar{q}_i(x_b) \left(\frac{d\hat{\sigma}_4}{dt} D_{q_i}^h(z) + \frac{d\hat{\sigma}_4}{du} D_{\bar{q}_i}^h(z) \right) + \bar{q}_i(x_a) q_i(x_b) \left(\frac{d\hat{\sigma}_4}{dt} D_{\bar{q}_i}^h(z) + \frac{d\hat{\sigma}_4}{du} D_{q_i}^h(z) \right) \right\} \quad . \quad (\text{A15})$$

$$\begin{aligned} \hat{\sigma}_4^{h-\bar{h}} : \quad & \sum_{q=u,d,s} [q(x_a) \bar{q}(x_b) - \bar{q}(x_a) q(x_b)] \left(\frac{d\hat{\sigma}_4}{dt} - \frac{d\hat{\sigma}_4}{du} \right) D_{q_V}^h(z) \\ &= \sum_{q=u,d,s} [q_V(x_a) q(x_b) - q(x_a) q_V(x_b)] \left(\frac{d\hat{\sigma}_4}{dt} - \frac{d\hat{\sigma}_4}{du} \right) D_{q_V}^h(z) \\ &= \sum_{q=u,d,s} [q_V(x_a) \bar{q}(x_b) - \bar{q}(x_a) q_V(x_b)] \left(\frac{d\hat{\sigma}_4}{dt} - \frac{d\hat{\sigma}_4}{du} \right) D_{q_V}^h(z) \\ &= \sum_{q=u,d,s} \frac{1}{2} [q_V(x_a) \tilde{q}(x_b) - \tilde{q}(x_a) q_V(x_b)] \left(\frac{d\hat{\sigma}_4}{dt} - \frac{d\hat{\sigma}_4}{du} \right) D_{q_V}^h(z) . \end{aligned} \quad (\text{A16})$$

$$\hat{\sigma}_4^{h+\bar{h}} : \quad \sum_{q=u,d,s} [q(x_a) \bar{q}(x_b) + \bar{q}(x_a) q(x_b)] \left(\frac{d\hat{\sigma}_4}{dt} + \frac{d\hat{\sigma}_4}{du} \right) D_q^{h+\bar{h}}(z) \quad (\text{A17})$$

5. $\hat{\sigma}_5: q_i \bar{q}_i \rightarrow gg$

$$\hat{\sigma}_5 : \quad \sum_{i=u,d,s} [q_i(x_a) \bar{q}_i(x_b) + q_i(x_b) \bar{q}_i(x_a)] \frac{d\hat{\sigma}_5}{dt} D_g^h(z) , \quad (\text{A18})$$

symmetric in $t - u$.

$$\hat{\sigma}_5^{h-\bar{h}} = 0 \quad (\text{A19})$$

$$\hat{\sigma}_5^{h+\bar{h}} : \quad \sum_{i=u,d,s} 2 [q_i(x_a) \bar{q}_i(x_b) + q_i(x_b) \bar{q}_i(x_a)] \frac{d\hat{\sigma}_5}{dt} D_g^h(z) , \quad (\text{A20})$$

6. $\hat{\sigma}_6: gg \rightarrow q_i \bar{q}_i$

$$\hat{\sigma}_6 : \quad g(x_a) g(x_b) \frac{d\hat{\sigma}_6}{dt} \sum_{i=u,d,s} [D_{q_i}^h(z) + D_{\bar{q}_i}^h(z)] , \quad (\text{A21})$$

symmetric in $t - u$.

$$\hat{\sigma}_6^{h-\bar{h}} = 0 \quad (\text{A22})$$

$$\hat{\sigma}_6^{h+\bar{h}} : \quad 2 g(x_a) g(x_b) \frac{d\hat{\sigma}_6}{dt} \sum_{i=u,d,s} D_{q_i}^{h+\bar{h}}(z) , \quad (\text{A23})$$

where we have used that C-inv. implies $D_g^h = D_g^{\bar{h}}$

7. $\hat{\sigma}_7: q_i g \rightarrow q_i g$

$$\hat{\sigma}_7 : \quad \sum_i \left\{ \left[(q_i(x_a) D_{q_i}^h + \bar{q}_i(x_a) D_{\bar{q}_i}^h) g(x_b) \frac{d\hat{\sigma}_7}{dt} + (q_i(x_a) + \bar{q}_i(x_a)) g(x_b) D_g^h \frac{d\hat{\sigma}_7}{du} \right] \right. \quad (\text{A24})$$

$$\left. + \left[(q_i(x_b) D_{q_i}^h + \bar{q}_i(x_b) D_{\bar{q}_i}^h) g(x_a) \frac{d\hat{\sigma}_7}{du} + (q_i(x_b) + \bar{q}_i(x_b)) g(x_a) D_g^h \frac{d\hat{\sigma}_7}{dt} \right] \right\} . \quad (\text{A25})$$

$$\hat{\sigma}_7^{h-\bar{h}} : \quad \sum_{q=u,d,s} \left\{ q_V(x_a) g(x_b) \frac{d\hat{\sigma}_7}{dt} + q_V(x_b) g(x_a) \frac{d\hat{\sigma}_7}{du} \right\} D_{q_V}^h. \quad (\text{A26})$$

$$\begin{aligned} \hat{\sigma}_7^{h+\bar{h}} : \quad & \sum_{q=u,d,s} \left\{ \left[\tilde{q}(x_a) g(x_b) \frac{d\hat{\sigma}_7}{dt} + \tilde{q}(x_b) g(x_a) \frac{d\hat{\sigma}_7}{du} \right] D_q^{h+\bar{h}} \right. \\ & \left. + 2 \left[\tilde{q}(x_a) g(x_b) \frac{d\hat{\sigma}_7}{du} + \tilde{q}(x_b) g(x_a) \frac{d\hat{\sigma}_7}{dt} \right] D_g^h \right\}. \end{aligned} \quad (\text{A27})$$

8. $\hat{\sigma}_8: gg \rightarrow gg$

$$\hat{\sigma}_8 : \quad g(x_a)g(x_b) \frac{d\hat{\sigma}_8}{dt} D_g^h(z), \quad (\text{A28})$$

symmetric in $t - u$.

$$\hat{\sigma}_8^{h-\bar{h}} = 0 \quad (\text{A29})$$

$$\hat{\sigma}_8^{h+\bar{h}} : \quad 2 g(x_a)g(x_b) \frac{d\hat{\sigma}_8}{dt} D_g^h(z), \quad (\text{A30})$$

The partonic cross sections that enter the difference cross sections, averaged over initial and summed over final spin and colour, are [9]:

$$\frac{d\hat{\sigma}_i(ab \rightarrow cd)}{dt} = \frac{\pi \alpha_s^2(Q^2)}{s^2} |M_i(s, t, u)|^2 \quad (\text{A31})$$

where the matrix elements $|M_i(s, t, u)|^2$ are:

$$|M_1(s, t, u)|^2 = \frac{4}{9} \frac{s^2 + u^2}{t^2} \quad (\text{A32})$$

$$|M_2(s, t, u)|^2 = \frac{4}{9} \left(\frac{s^2 + u^2}{t^2} + \frac{s^2 + t^2}{u^2} \right) - \frac{8}{27} \frac{s^2}{tu} \quad (\text{A33})$$

$$|M_4(s, t, u)|^2 = \frac{4}{9} \left(\frac{s^2 + u^2}{t^2} + \frac{u^2 + t^2}{s^2} \right) - \frac{8}{27} \frac{u^2}{st} \quad (\text{A34})$$

$$|M_7(s, t, u)|^2 = -\frac{4}{9} \frac{s^2 + u^2}{us} + \frac{s^2 + u^2}{t^2}. \quad (\text{A35})$$

-
- [1] D. de Florian, R. Sassot, M. Epele, R. J. Hernández-Pinto, and M. Stratmann, Phys. Rev. D **91**, 014035 (2015), 1410.6027.
 - [2] D. de Florian, M. Epele, R. J. Hernandez-Pinto, R. Sassot, and M. Stratmann, Phys. Rev. D **95**, 094019 (2017), 1702.06353.
 - [3] E. Leader, A. V. Sidorov, and D. B. Stamenov, Phys. Rev. D **93**, 074026 (2016), 1506.06381.
 - [4] M. Hirai, S. Kumano, T. H. Nagai, and K. Sudoh, Phys. Rev. D **75**, 094009 (2007), hep-ph/0702250.
 - [5] S. Albino, B. A. Kniehl, and G. Kramer, Nucl. Phys. B **803**, 42 (2008), 0803.2768.
 - [6] B. Jager, A. Schafer, M. Stratmann, and W. Vogelsang, Phys. Rev. D **67**, 054005 (2003), hep-ph/0211007.
 - [7] B. L. Combridge, J. Kripfganz, and J. Ranft, Phys. Lett. B **70**, 234 (1977).
 - [8] R. Cutler and D. W. Sivers, Phys. Rev. D **17**, 196 (1978).
 - [9] J. F. Owens, E. Reya, and M. Gluck, Phys. Rev. D **18**, 1501 (1978).
 - [10] R. P. Feynman, R. D. Field, and G. C. Fox, Phys. Rev. D **18**, 3320 (1978).
 - [11] R. Baier, J. Engels, and B. Petersson, Z. Phys. C **2**, 265 (1979).
 - [12] R. K. Ellis, M. A. Furman, H. E. Haber, and I. Hinchliffe, Nucl. Phys. B **173**, 397 (1980).
 - [13] R. K. Ellis and J. C. Sexton, Nucl. Phys. B **269**, 445 (1986).
 - [14] F. Aversa, P. Chiappetta, M. Greco, and J. P. Guillet, Nucl. Phys. B **327**, 105 (1989).
 - [15] J. Adams et al. (STAR), Phys. Lett. B **637**, 161 (2006), nucl-ex/0601033.
 - [16] B. I. Abelev et al. (STAR), Phys. Rev. C **75**, 064901 (2007), nucl-ex/0607033.
 - [17] G. Agakishiev et al. (STAR), Phys. Rev. Lett. **108**, 072302 (2012), 1110.0579.

- [18] J. Pumplin, D. R. Stump, J. Huston, H. L. Lai, P. M. Nadolsky, and W. K. Tung, JHEP **07**, 012 (2002), hep-ph/0201195.
- [19] E. Christova and E. Leader, Phys. Rev. D **79**, 014019 (2009), 0809.0191.
- [20] C. Bourrely, J. Soffer, and F. Buccella, Phys. Lett. B **648**, 39 (2007), hep-ph/0702221.
- [21] K. Adcox et al. (PHENIX), Phys. Rev. Lett. **88**, 022301 (2002), nucl-ex/0109003.
- [22] J. Adams et al. (STAR), Phys. Rev. Lett. **92**, 112301 (2004), nucl-ex/0310004.
- [23] V. Kekelidze, V. Kolesnikov, V. Matveev, and A. Sorin, Springer Proc. Phys. **250**, 503 (2020).
- [24] A. Taranenko, J. Phys. Conf. Ser. **1685**, 012021 (2020).
- [25] H. Torii (PHENIX), Nucl. Phys. A **715**, 753 (2003), nucl-ex/0210005.
- [26] P. Aurenche, T. Binoth, M. Fontannaz, J.-P. Guillet, G. Heinrich, E. Pilon, and M. Werlen, https://lapth.cnrs.fr/PHOX_FAMILY/readme_inc.html.
- [27] J. Pumplin, D. Stump, R. Brock, D. Casey, J. Huston, J. Kalk, H. L. Lai, and W. K. Tung, Phys. Rev. D **65**, 014013 (2001), hep-ph/0101032.
- [28] M. Demirci and A. I. Ahmadov, Int. J. Mod. Phys. A **33**, 1850166 (2018), 1810.01491.
- [29] L. Adamczyk et al. (STAR), Phys. Rev. C **96**, 044904 (2017), 1701.07065.
- [30] B. I. Abelev et al. (STAR), Phys. Rev. Lett. **97**, 152301 (2006), nucl-ex/0606003.
- [31] B. I. Abelev et al. (STAR), Phys. Rev. C **79**, 034909 (2009), 0808.2041.
- [32] G. Antchev et al. (TOTEM), Eur. Phys. J. C **79**, 103 (2019), 1712.06153.
- [33] L. Apanasevich, M. Begel, C. Bromberg, T. Ferbel, G. Ginther, J. Huston, S. E. Kuhlmann, P. Slattery, M. Zielinski, and V. Zutshi, Phys. Rev. D **63**, 014009 (2001), hep-ph/0007191.
- [34] L. Apanasevich et al. (Fermilab E706), Phys. Rev. D **68**, 052001 (2003), hep-ex/0204031.
- [35] F. W. Busser et al., Nucl. Phys. B **106**, 1 (1976).